Contrasting physical erosion rates in cratonic catchments: the Ogooué and Mbei rivers, Western Central Africa

V. Regard, Sebastien Carretier, Jean-Sébastien Moquet, S. Choy, P.-H. Blard, S. Bogning, A.P. Mbonda, E. Mambela, M.C. Paiz, M. Séranne, et al.

Contrasting physical erosion rates in cratonic catchments: the Ogooué and Mbei rivers, Western Central Africa

V. Regard[1,*], S. Carretier[1], J.-S. Moquet[2], S. Choy[1], P.-H. Blard[3,4], S. Bogning[5], A. P. Mbonda[6], E. Mambela[7], M. C. Paiz[7], M. Séranne[8], J. Charreau[3], D. Rouby[1], J. Bouchez[9], J. Gaillardet[9], J.-J. Braun[1,10,11], Y. Denèle[1]

1. GET (Université de Toulouse, CNRS, IRD, UPS, CNES), Toulouse, France

2. Univ. Orléans, CNRS, BRGM, ISTO, UMR 7327, F-45071, Orléans, France

3. CRPG, CNRS, Université de Lorraine, Nancy, France

4. Laboratoire de Glaciologie, ULB, Brussels, Belgium

5. Université de Douala, Cameroon

6. Centre National de la Recherche Scientifique, Libreville, Gabon

7. The Nature Conservancy, Libreville, Gabon

8. Géosciences Montpellier, Université de Montpellier, CNRS, Montpellier, France

9. IPGP (Université Paris Cité, CNRS, Université La Réunion, IGN), Paris, France

10. LMI DYCOFAC IRD-University of Yaoundé 1-IRGM, BP 1857 Cameroon

11. Agence Nationale des Parcs Nationaux, Libreville, Gabon

* Corresponding author. Vincent.regard@get.omp.eu, +33 561332645, 14 av. Edouard Belin, 31400 Toulouse, France

Bullet points

- The Ogooué River catchment is denuding at a low rate (38 t/km^2/a, 15 m/Ma)
- There is substantial chemical denudation: > 30% of the total denudation
- Batéké Px not producing solutes because constituted by already weathered material
- The southern part of the catchment is denuding twice as fast as the northern part
- Landscape seems close to equilibrium: chemical proportional to physical denudation

Abstract

We measured the long-term physical denudation of the Ogooué River catchment using ^{10}Be produced in situ by cosmic rays. These measurements are averaged over 25-200 ka (average 40 ka), depending on the physical denudation rate. The denudation rate of the Ogooué River catchment is slow (38 t/km^2/a, 15 m/Ma), slightly higher than in Equatorial West Africa (from Senegal to Angola, 26 t/km^2/a, 10 m/Ma). Physical denudation and chemical weathering fall within the same order of magnitude. Thus, although low, there is substantial chemical weathering compared to physical denudation, that likely contributes over 30% of the total denudation.

Denudation rates are spatially variable (from 10 to 60 t/km^2/a) within the large Ogooué River catchment. Over the long term, physical denudation and chemical weathering roughly match, except in the Batéké Plateaux area, because the plateaus are made up of already weathered detrital material and therefore their modern flux of solutes is very low (~9.5 t/km^2/a). The spatial distribution is similar to the one described in the work of Moquet et al. (2021) on the basis of solute fluxes, i.e. the southern part of the catchment is denuding twice as fast as the northern part. We show here that the whole picture did not vary much since 100 ka, as shown by both methods which give consistent results. Faster

denudation in the southern part of the catchment may be related to more uplift than in the northern part caused by the southern African “superswell”.

Keywords

Cosmogenic nuclides; denudation; chemical weathering; cratonic areas; Ogooué River

1 Introduction

There is still active debate today on the role of mountains in: (1) global erosion, (2) denudation fluxes, and (3) the production of sediments exported to the ocean (e.g. Willenbring et al., 2013; Larsen et al., 2014; Maffre et al., 2018). Although relatively slow (~120 t/km^2/a, equivalent to 45 m/Ma), the denudation of flat continental regions (slope < 200 m/km) results in a significant contribution of sediments to global fluxes given the vast areas involved (Willenbring et al., 2013). Cratonic areas only account for approximately 15% (according to Şengör et al., 2022) of the catchment-wide denudation rates measured through the cosmogenic isotope ^{10}Be on detrital sands (from the Octopus database, Codilean et al., 2018). Although a significant body of literature has attempted to identify the controls on denudation rates in tectonically actives areas (e.g. Burbank et al., 1996; Galy and France-Lanord, 2001; Carretier et al., 2013; Godard et al., 2014; Scherler et al., 2017), there are very few similar studies in tectonically inactive regions where mass wasting and faulting are rare.

The Ogooué River Basin (ORB) in Gabon, located in Equatorial Africa, (Figure 1) is particularly suitable for studying the denudation of such tectonically inactive (or low activity) areas since it drains a relatively large area that is representative of the cratonic zones of Equatorial and Tropical West Africa (along the Atlantic coast from Senegal to Angola) and it is underlain by a relatively homogeneous

lithology. The catchment is relatively pristine from the perspective of long-term denudation processes and rates, as anthropic pressure has increased only recently.

In the present study, we quantify the catchment-scale denudation rates in nested watersheds across the ORB using *in situ* cosmogenic nuclide measurements on river sands (Figure 2). However, because of thick regolith layers, cosmogenic nuclide measurements in cratonic areas only record physical denudation, as this method is blind to chemical denudation that occurs deeper than 1 m below the surface (Figure 3) (Riebe et al., 2003; Granger and Riebe, 2007; Dixon et al., 2009; Hewawasam et al., 2013; Regard et al., 2016). We use chemical denudation estimates for the Ogooué River Basin at the same sites as by Moquet et al. (2021) in order to obtain estimates of the total denudation rates. Our data allow us to quantify the denudation, to estimate the contribution of physical *vs*. chemical processes to the total denudation, and to produce a spatially distributed estimate of these rates within the ORB, providing an opportunity to identify the underlying controls on denudation in this tectonically inactive region.

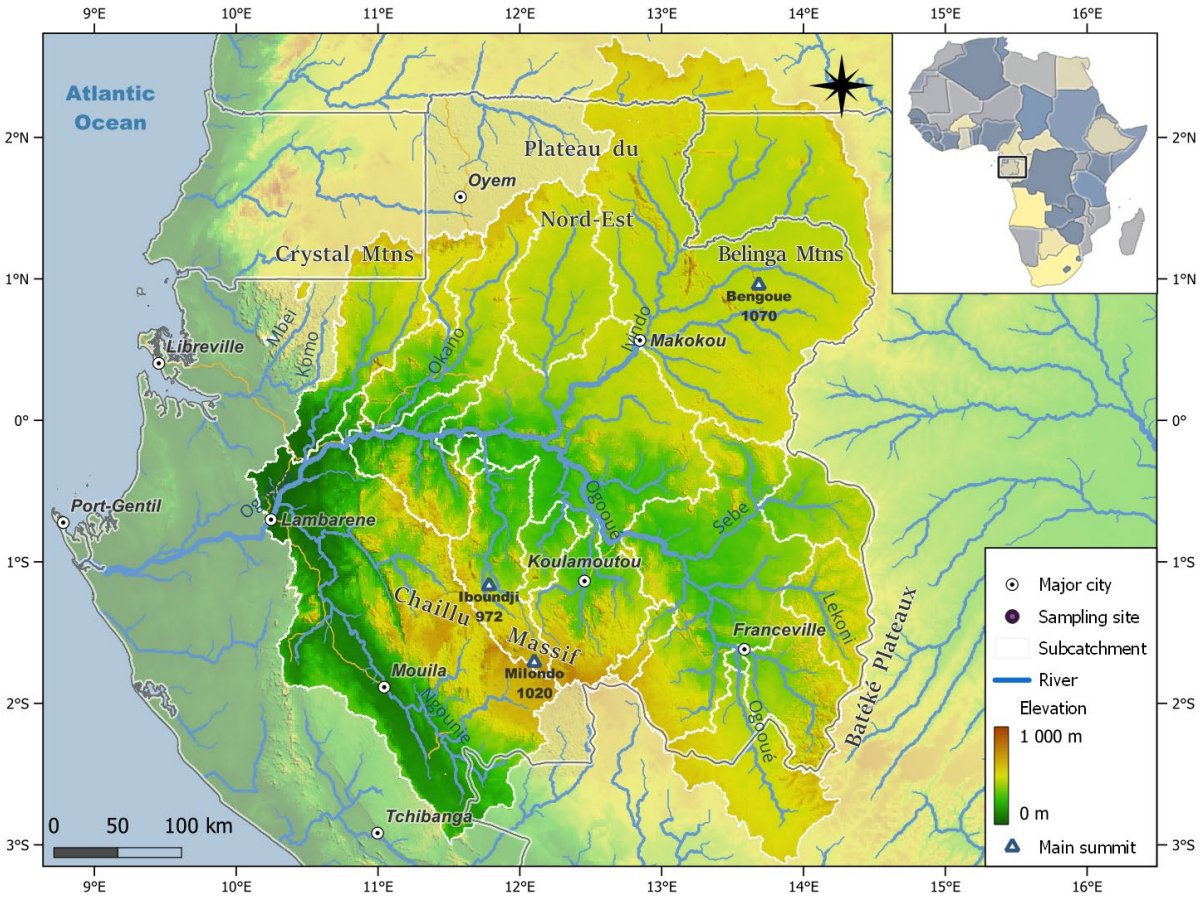

79

80 *Figure 1. (Inset) map showing the location of the Ogooué river basin (ORB) in Central West Africa. The main map shows the*

81 *relief, hydrographic network of the Ogooué River, and sampling locations* (figure taken from Moquet et al., 2021). *The Mbei*

82 *catchment sampling points are indicated to the north-east.* [Printed in Black & White]

83

84

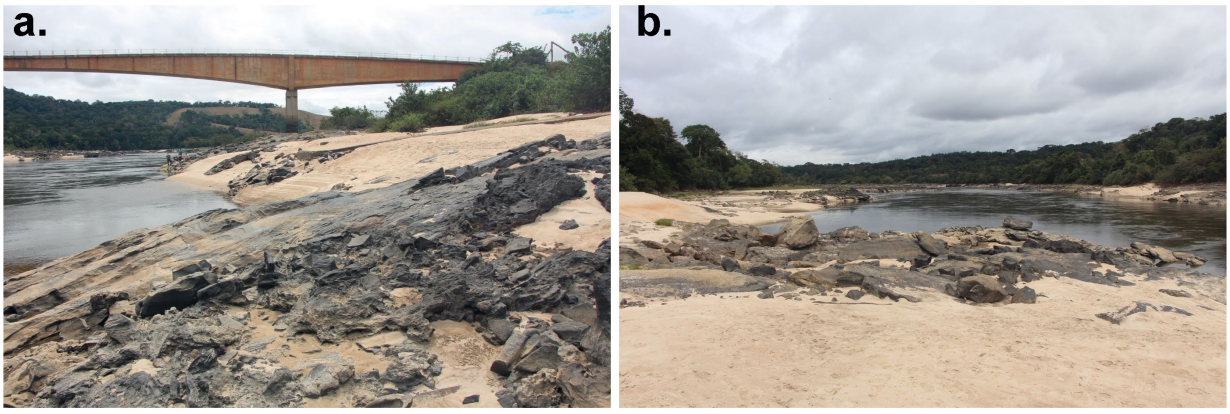

85

Figure 2. Photos of the sampling sites along the Ogooué River at Ayem (sampling site #26), upstream (note the people for scale) and downstream. Sand was sampled from the banks at this site. [Printed in Black & White]

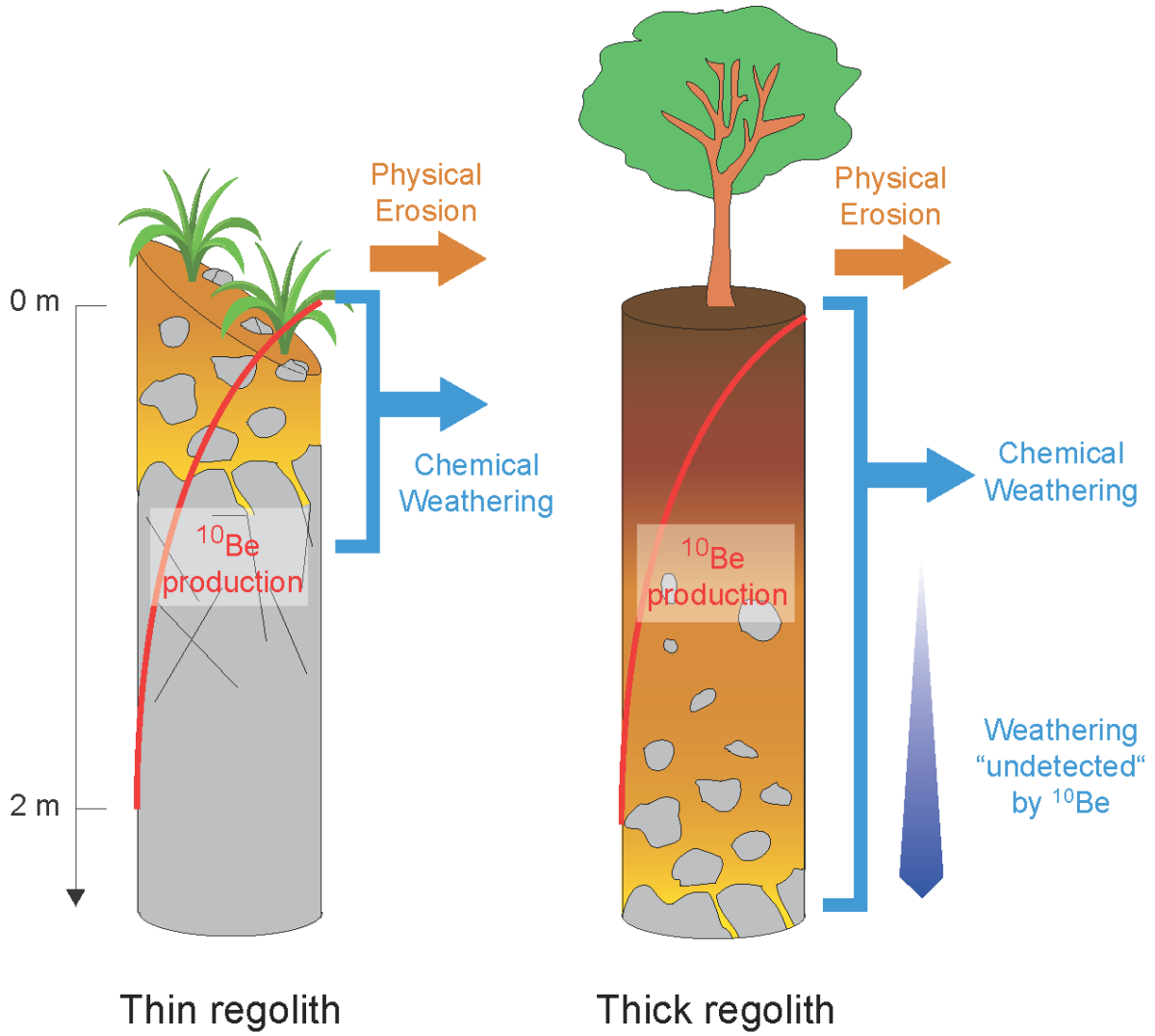

Figure 3. *Sketch showing the difference in how chemical weathering is detected by cosmogenic isotopes in the case of a thin (left) vs. thick (right) regolith. Cosmogenic isotope production is high at the surface and decreases rapidly at depth (on a meter scale, as shown in the figure). Thus, the rate of denudation detected by cosmogenic isotopes relates to processes taking place less than around one meter below the surface. If the regolith is thin, then the cosmogenic-derived denudation rate includes both physical and chemical denudation. If the regolith is thick, then cosmogenic isotopes only "see" a part of the chemical denudation, as some of it takes place too deep.*

2 Study area

The equatorial Ogooué River Basin (ORB) spans ~220,000 km², from 9 to 14°E and 2.5°N to 3°S (Figure 1), across the countries of Gabon (85% of the catchment), Congo (12%) and Equatorial Guinea and Cameroon (Figure 1). The river discharge at the mouth is ~4,750 $m^3.s^{-1}$ (Bogning et al., 2018), corresponding to roughly 10% of the neighboring Congo River, the largest river in Africa (discharge ~41,000 $m^3.s^{-1}$; catchment area 3.7×10^6 km^2) (Laraque et al., 2009).

The climate in the Ogooué catchement is tropical *sensu* Köppen-Geiger with one dry season from June to August (Kottek et al., 2006) and with a bimodal precipitation regime with wet periods from March to May and October to December. The average yearly rainfall is approximately 2,000 $mm.a^{-1}$ leading to a runoff of 700 $mm.a^{-1}$ (Bogning et al., 2018; Kittel et al., 2018). The average temperature is constant throughout the year, ~24°C.

The study area corresponds to 96% of the Ogooué catchment upstream from the Lambaréné station (206,000 km², sampling point OG-05, Figure 1). In addition, we sampled four tributaries of the Mbei River, a tributary of the neighboring Komo River in Northern Gabon which drains terrains that are similar to those underlying the ORB (Figure 1). The annual discharge of the Mbei River is ~60 $m^3.s^{-1}$ over an area extending ~ 1,800 km^2 (ORSTOM, 1964; Njutapvoui Fokouop, 2017 data for the period 1964-1973 only). The four monitored Mbei tributaries cover an area of less than 500 km². There, rainfall is ~2000 $mm.a^{-1}$ and runoff ~600 $mm.a^{-1}$.

Geologically speaking, most of the Ogooué River Basin is developed within plutonic and meta-plutonic rocks of the Archean Congo Craton, affected by the Eburnean orogeny in the Paleoproterozoic (Thiéblemont et al., 2009a, 2009b). The lithology of these rocks is predominantly dominated by granites and granitoids, although bands of high-grade metamorphic meta-sedimentary rocks are locally observed, such as the Meso- to Neo-Archean schists and metaconglomerates of the Bélinga Group or the Paleoproterozoic schists of the N'Dolé Group, as well as the Paleoproterozoic micaschists

and paragneisses of the Ogoué Complex (Figure 4). In the southeast, the upstream parts of the basin are located at the Western termination of the Batéké Plateaux, mostly composed of purely quartzitic Cenozoic sandstone (Séranne et al., 2008), and in predominantly detrital sedimentary rocks (pelites, sandstones, and conglomerates) of the Paleoproterozoic Francevillian basins. The sandstone formation of the Batéké Plateaux, discordant on the crystalline basement, is located close to the border with the Congo, where the existence of significant Neogene uplift has been shown, possibly related to mantle swell (Al-Hajri et al., 2009; Guillocheau et al., 2015; Weber et al., 2016). The western and downstream parts of the Ogooué River Basin have mainly developed within the northern termination of the Neoproterozoic orogenic belt of western Congo and in the coastal basin with Phanerozoic lithostratigraphy. In this sector, lithologies are more diverse, with carbonate formations alternating with predominantly fine-grained detrital formations (sandstones and argillites). In summary, the northern tributaries of the Ogooué catchment, as well as the Mbei catchment, exclusively drain Archean cratonic rocks. The southern tributaries drain both Archean cratonic rocks and Neoproterozoic volcano-sedimentary rocks. The main Ogooué channel drains Quaternary fluvial sediments in addition to the Mesozoic - Cenozoic basin in its downstream part and the Archean basement in its upstream part Paleoproterozoic Francevilian metasediments in Boumango area) (Thiéblemont et al., 2009a, 2009b) All these lithologies are quartz-rich and are covered by 2- to 3 ka-old, 1-3 m-thick, clayey to sandy laterite-derived aeolian products and regionally known as the “Cover Horizon” (Thiéblemont et al., 2009a).

The elevation of the Ogooué catchment ranges from 20 m.a.s.l. (Lambaréné station) to ~1000 m.a.s.l. (Figure 1); the elevation of the Mbei catchments ranges from 130 to 800 m.a.s.l. The slopes of the Ogooué catchment are low, (~1°), whereas the areas drained by the Mbei tributaries upstream from our sampling sites are steeper, with average slopes up to 7-8° (Moquet et al., 2021).

Following the information provided above, the sampling points and respective catchments are grouped into five areas: (1) the Batéké Plateaux, (2) the northern Ogooué tributaries, (3) the southern Ogooué tributaries, (4) the Ogooué main channel, where fluxes are averaged over catchments from

147 the first three categories, and (5) the Mbei River tributaries. The characteristics of these domains are
148 summarized in Table 1.

149 *Table 1. Characteristics of the various areas studied.*

150

	Batéké Plateaux	Southern tributaries	Northern tributaries	Main Ogooué	Mbei tributaries
Lithology (rocks)	Quartz sandstone	Plutonic, metaplutonic and metasedimentary, volcano-sedimentary	Plutonic, metaplutonic, and metasedimentary rocks	Plutonic, metaplutonic and metasedimentary, volcano-sedimentary, quartz sandstones, limestones	Plutonic, metaplutonic and metasedimentary
Elevation (m)	300-800	150-1100	150-1100	150-1100	150-750
Average slope (%)	0.8-2	1.3-2	0.5-3	0.5-1.5	1-8
Av. rainfall ($mm.a^{-1}$)	2300-2700	1900-2600	~1900	2100-2600	1900-2300
Vegetation	Extensive agriculture and savanna	Forest	Forest	Forest	Forest
^{10}Be denudation rate (m/Ma and $t/km^2/a$)	7-22 m/Ma 20-60 $t/km^2/a$	8-20 m/Ma 21-51 $t/km^2/a$	3-8 m/Ma 8-22 $t/km^2/a$	7-18 m/Ma 19-48 $t/km^2/a$	6-23 m/Ma 15-60 $t/km^2/a$
Modern TDS flux (Moquet et al. 2021)	8-12 $t/km^2/a$	30-53 $t/km^2/a$	11-22 $t/km^2/a$	15-20 $t/km^2/a$	14-18 $t/km^2/a$

151

152 3 Material and methods

153 3.1 Sampling

154 We collected 22 river sand samples in September 2017: five samples in the Ogooué main channel, 13
155 samples in the Ogooué's tributaries and four samples in the Mbei River and tributaries (Figure 4 and
156 Table 2). Three additional samples (labelled BTK) were collected previously during another campaign
157 in January and February 2008: BTK08-22 on the main Ogooué River upstream (just upstream of sample
158 OG-17 from the 2017 campaign); BTK08-5 from the Léconi River, a tributary of the Ogooué, collected
159 at a location very close to sample OG-15 from 2017; and BTK08-20 from the Socle River, a southern
160 tributary of the Ogooué, quite close to the 2017 OG-19 sample on the Leyou, where the river only
161 drains Archean plutonic rocks. Approximately 1 kg of sand was collected at each sampling point from
162 recently deposited riverbanks. The sampled sands consist almost entirely of quartz, as commonly

observed for lowland tropical rivers, making it easy to carry out the chemical treatment described below.

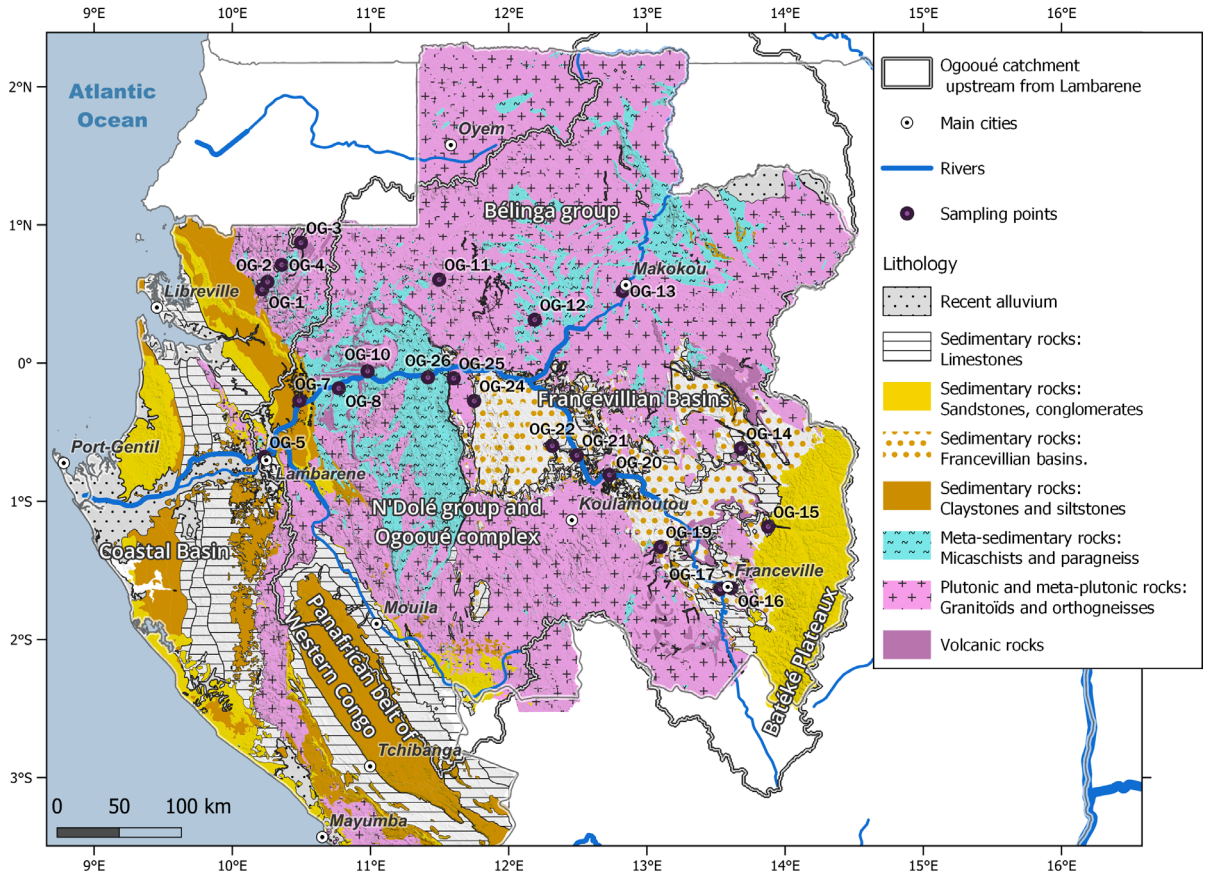

Figure 4. Lithological map of Gabon (Thiéblemont et al., 2009b) *with our sampling sites and the Ogooué catchment. The area comprising the metamorphic and plutonic rocks is part of the Congo Craton.* [Printed in Black & White]

3.2 Measurement of the in-situ ^{10}Be concentrations

All samples were processed for *in situ* beryllium-10 (^{10}Be) at GET (Géosciences Environnement Toulouse), with the exception of samples BTK08-5, BTK08-20 and BTK08-22 which were processed at CRPG (Centre de Recherches Pétrographiques et Géochimiques, Nancy) for both ^{10}Be and aluminium-26 (^{26}Al), following the procedure described in Puchol et al. (2017).

The samples were first sieved to extract the 500-1000 µm size fraction, which then underwent a series of acid attacks with a mixture of concentrated hydrochloric (HCl) and hexafluorosilisic (H_2SiF_6) acids to

remove all non-quartz minerals. Meteoric ^{10}Be was then removed by three partial leaching steps with concentrated hydrofluoric acid (HF). The leached quartz was dissolved with concentrated hydrofluoric acid (HF) after adding a ^{9}Be carrier solution (500 µL of a [^{9}Be] = 1000 µg/g solution for the GET batch, and 100 mg of a [^{9}Be] = 3066 µg/g solution for the CRPG batch). The resulting solutions were evaporated until dryness and the samples were recovered with hydrochloric acid. Dissolved species were then precipitated with concentrated ammonia before processing through an anion exchange column to remove the iron, and a cation exchange column to discard the boron and recover Be (as well as Al for two samples processed at CRPG). After elution, Be was precipitated as $Be(OH)_2$ by adding concentrated ammonia at pH = 8 and oxidized to BeO. After preparing the target by mixing niobium powder with the BeO oxide, the ^{10}Be/^{9}Be ratios were measured by Accelerator Mass Spectrometry (AMS) at the French National AMS Facility ASTER of CEREGE in Aix-en-Provence (Arnold et al., 2010). In the case of the GET batch, the measured ^{10}Be/^{9}Be ratios were calibrated against an in-house standard STD-11 with an assigned value of $(1.191 \pm 0.013) \times 10^{-11}$ (Braucher et al., 2015), while the CRPG batch was calibrated against the SRM 4325 NIST reference material, using a ^{10}Be/^{9}Be ratio of $(2.79 \pm 0.03) \times 10^{-11}$ (Nishiizumi et al., 2007). Both are similar to the KNSTD07 calibration (Balco et al., 2008; Nishiizumi et al., 2007). The analytical 1σ uncertainties include uncertainties in the AMS counting statistics, the uncertainty in the standard ^{10}Be/^{9}Be ratio, an external AMS error of 0.5% (Arnold et al., 2010), and a chemical blank correction (that yielded ^{10}Be/^{9}Be ratios of $(9.9 \pm 0.6) \times 10^{-15}$, $(9.8 \pm 0.6) \times 10^{-15}$, and $(2.1 \pm 1.0) \times 10^{-15}$ for the first GET, second GET, and CRPG batches, respectively; Table 2). A ^{10}Be half-life of 1.387 ± 0.01 Ma was used (Chmeleff et al., 2010; Korschinek et al., 2010)

For the specific case of the samples processed for the ^{26}Al measurements, the ^{27}Al concentrations were measured from small aliquots of the dissolved samples, after evaporation and substitution of fluorides by HNO_3. This measurement was done by inductively coupled plasma optical emission spectrometry (ICP-OES) at the Service National d'Analyse des Roches et Minéraux (SARM, CRPG, Vandoeuvre, France). The ^{26}Al/^{27}Al ratios measured at ASTER were normalized to the ASTER in-house standard SM-

202 Al-11, with a $^{26}Al/^{27}Al$ value of $(7.40 \pm 0.06) \times 10^{-12}$. The analytical $^{26}Al/^{27}Al$ blank ratio was $(3 \pm 3) \times 10^{-}$

203 ^{15}.

204 *Table 2. ^{10}Be and ^{26}Al analytical data. The uncertainties are 1σ. See text for methods and calibrations.*

205

206

207

Sample name	Sample code	Location	River	Latitude	Longitude	Elevation	Domain	Dissolved Quartz	^{9}Be added through carrier	Uncertainty	Measured ^{10}Be/ ^{9}Be	Uncertainty	^{10}Be	Uncertainty	^{27}Al content	Uncertainty	Measured ^{26}Al/ ^{27}Al	Uncertainty	^{26}Al	Uncertainty
				(°N)	(°E)	(m asl)		(g)	(10^{15} at)		(x 10^{15})	(%)	(at/g)		(10^{15} at)		(x 10^{-15})	(%)	(at/g)	
First series of samples†																				
OG-01	**01**			0.5332	10.2148	139	Mbei	20.96	34 194	102	58	4.34%	94 690	3 374						
OG-02	**02**	Akelayong	Mbei	0.5874	10.2541	160	Mbei	20.85	34 167	102	218	2.77%	357 636	9 126						
OG-03	**03**	Akoga	Mwenge	0.8709	10.4961	534	Mbei	20.79	34 067	101	223	2.62%	365 831	8 814						
OG-04	**04**	Assok	Binguili	0.7110	10.3570	526	Mbei	19.46	34 180	102	163	3.19%	287 148	8 320						
OG-05	**05**	Lambaréné	Ogooué	-0.6804	10.2313	2	Ogooué main channel	20.91	33 993	101	92	3.86%	150 272	5 031						
OG-07	**07**	Abanga	Abanga	-0.2726	10.4847	16	Northern tributaries	20.47	34 046	101	160	3.62%	266 179	8 833						
OG-08	**08**	Ndjolé	Ogooué	-0.1827	10.7701	16	Ogooué main channel	19.70	34 267	102	85	4.27%	148 466	5 519						
OG-10	**10**	Alembé	Ogooué	-0.0591	10.9782	46	Northern tributaries	20.18	34 040	101	204	3.57%	343 595	11 444						
OG-11	**11**	Mindzi	Lara	0.6034	11.4966	313	Northern tributaries	20.22	34 160	102	278	3.38%	470 474	15 072						
OG-12	**12**	Ovan	Mvoung	0.3136	12.1879	404	Northern tributaries	20.12	34 046	101	260	2.56%	439 423	10 469						
OG-13	**13**	Loaloa	Ivindo	0.5215	12.8245	462	Northern tributaries	20.04	34 153	102	442	2.28%	752 413	16 405						
OG-14	**14**	Okandja	Sébé	-0.6176	13.6812	295	Batéké Plateaux	12.87	33 933	101	61	4.07%	161 295	5 384						
OG-15	**15**	Akieni	Léconi	-1.1852	13.8773	387	Batéké Plateaux	22.22	34 060	101	217	2.79%	332 742	8 575						
OG-16	**16**	Franceville	Passa	-1.6294	13.6103	287	Batéké Plateaux	22.66	33 384	99	69	4.20%	101 983	3 604						
Chemical blank									33 993	101	9.92	5.58%								
Second series of samples†																				
OG17	**17**	Franceville	Ogooué	-1.6355	13.5314	285	Ogooué main channel	21.26	34 060	101	209	3.39%	334 443	10 475						
OG19	**19**	Ndoubi	Leyou	-1.3313	13.0989	293	Southern tributaries	23.67	34 127	102	91	4.08%	131 902	4 614						
OG20	**20**	Lastourville	Ogooué	-0.8096	12.7285	228	Ogooué main channel	22.38	33 873	101	85	3.99%	127 982	4 312						
OG21	**21**	Lolo	Lolo	-0.6685	12.4929	213	Southern tributaries	19.80	33 919	101	71	4.24%	121 210	4 256						
OG22	**22**	Wagny	Ouagna	-0.5988	12.3150	201	Southern tributaries	24.14	33 411	99	150	3.70%	207 510	6 925						
OG24	**24**	Parc Lopé	Offoué	-0.2744	11.7502	145	Southern tributaries	21.35	34 107	101	100	4.27%	160 380	5 981						
OG25	**25**	Lopé	Offoué	-0.1102	11.6019	118	Southern tributaries	19.90	34 127	102	146	3.49%	251 038	7 836						
OG26	**26**	Ayem	Ogooué	-0.1037	11.4153	88	Ogooué main channel	22.39	34 046	101	83	3.96%	126 564	4 222						
Chemical blank									33 859	101	9.75	6.39%								
Third series of samples‡																				
BTK08-5	**08-5**	Akiéni	Léconi	-1.1801	13.8917	440	Batéké Plateaux	25.98	20 425		130	3.77%	206 160	7 766	33 551	554	670	4.78%	864 754	41 310
BTK08-20	**08-20**	Bakoumba	Socle	-1.8633	13.0138	537	Southern tributaries	18.93	20 685		146	3.09%	126 577	3 907						
BTK08-22	**08-22**	Poubara	Ogooué	-1.7623	13.5450	395	Ogooué main channel	30.41	20 359		94	3.09%	321 498	9 948	25 955	636	1 257	3.07%	1 722 966	52 842
Chemical blank											2.1	47.62%					3	100%		

3.3 Calculation of the ^{10}Be-derived, catchment-wide denudation rates

The catchment-scale denudation rates were calculated neglecting the radioactive decay, as per Lupker et al. (2012):

$$\bar{\varepsilon} = \frac{P_n\mu_n + P_{sm}\mu_{sm} + P_{fm}\mu_{fm}}{\rho[CN]}$$

where $\bar{\varepsilon}$ is the mean denudation rate in cm/a; ρ is the rock density (= 2.7 g/cm^3); [CN] is the cosmogenic nuclide concentration (at/g); P_n, P_{sm} and P_{fm} (at/g/a) are the catchment average cosmogenic nuclide production rates by neutrons, slow muons, and fast muons, respectively, and μ_n, μ_{sm} and μ_{fm} (g/cm^2) are the attenuations for neutrons, slow muons, and fast muons, respectively. The average ^{10}Be production rates for each cosmogenic production pathway were calculated using a cell-by-cell approach and the Basinga GIS toolbox (Charreau et al., 2019). In this toolbox, the mean sea surface level high latitude (SLHL) production rate is 4.18 at/g (Martin et al., 2017) and includes 98.86%, 0.27% and 0.87% atoms produced by neutrons, slow muons and fast muons, respectively (Martin et al., 2017 after; Braucher et al., 2011). From this SLHL value, the ^{10}Be production rates were calculated for each pixel (90 m resolution, from a SRTM 3 arc-seconds DEM) of the catchment area overlying a quartz-hosting lithology, scaled for latitude (neutrons only) and elevation (neutrons and muons) using the scaling models of Stone (2000) and the ERA-40 atmosphere atlas (Uppala et al., 2005). Following the recommendation from DiBiase (2018), no topographic shielding factor was applied. All pixel values were then averaged within each catchment to determine P_n, P_{sm}, and P_{fm}. The denudation rate uncertainty was calculated by propagating the analytical uncertainty on [CN] and a 15% uncertainty on the production rates. To test for the possibility of a bias associated with the abundance of quartz, variable quartz percentages were assigned to the different lithologies present in this catchment. The ^{10}Be production rates are weighted by these quartz percentages according to Carretier et al. (2015). The resulting denudation rates are within 1.5% equal to those calculated with a constant quartz

abundance, reported in Table 3. We estimate that for denudation rates of between 8 and 30 m/Ma, neglecting radioactive decay only results in an overestimate between 15 and 5% of the denudation rate, which remains within the uncertainty associated with the assumed uncertainty of 15% for the production rate.

The time over which cosmogenic nuclides are averaging catchment-wide erosion rates is called the integration time (τ). It corresponds to the time required to remove one attenuation length ($L = \mu_n/\rho$ [cm]) from the Earth surface. For this calculation, only spallation by neutrons is considered: $\tau = L/\bar{\varepsilon}$. It should be noted that this method captures all the denudation processes that take place close to the surface (max depth ~L), so we use the term denudation. To calculate the total denudation, i.e. taking the deeper weathering processes into account, it is necessary to use independent measurements of weathering rates or to make necessary assumptions, which will be the subject of section 4.3.

It should be noted that the "Cover Horizon" has probably disturbed the steady-state condition necessary for the use of cosmogenic nuclides to measure denudation rates. However, as this perturbation is very recent, we can assume, following Ferrier and Kirchner (2008), that the denudation rate evaluation is robust to such a small deviation from the steady state. This is further illustrated by the fact that the integration time (τ) is much larger than the age of the cover horizon (2-3 ka).Chemical denudation rates

Our sampling sites in the ORB are constrained for total dissolved solids (TDS) by the study of Moquet et al. (2021), which enables the estimation of the chemical denudation rates when used in combination with long-term water discharge estimates. However, because the river hydrochemistry at the sampling sites has only been measured once, the relevance of the calculated solute fluxes might be questioned in terms of long-term denudation, due to variable solute concentrations over a one year period. Moquet et al. (2021) noted that in other West African rivers such as the Nyong (Viers et al., 2000), Niger (Picouet et al., 2002) and Congo (Laraque et al., 2009), the TDS concentration varies only slightly with discharge over the year, meaning that solute fluxes in these rivers are mainly controlled by discharge variability, thereby lending confidence to the solute flux estimates based on the

hydrochemistry measured during a single sampling campaign. The propagation of various sources of uncertainties, which include the single point sampling strategy, has been estimated and described by Moquet et al. (2021, section 3.7 “Uncertainty calculation”). Therefore, the uncertainties associated with the chemical weathering flux used in the present paper includes this source of uncertainty. The long-term discharge (multi-year) at the sampling sites was estimated through a statistical approach based on a regional polynomial regression between specific discharge (Q_{spe}) and rainfall (P) (see Moquet et al., 2021 for details). As outlined by Moquet et al. (2021), we can reasonably consider that the studied rivers tend to exhibit a so-called “chemostatic behavior” which indicates that, despite the fact that some variability in the solute concentration exists, a single sampling point in space can be used to produce reasonable, first-order estimates of catchment-scale weathering rates.

In the ORB, most of the river solute flux is derived from silicate chemical weathering; < 15% is derived from atmospheric inputs (Moquet et al., 2021). Low cationic weathering rates are observed for the Batéké Plateaux (TZ_{sil}^+ ~0.5 t/km^2/a, where TZ_{sil}^+ represents the chemical weathering rate expressed as the release rate of the sum of cations by silicate chemical weathering). Higher weathering rates are typical of the southern catchments (TZ_{sil}^+ ~3.4 t/km^2/a), and intermediate rates (TZ_{sil} between 1.7 and 2.5 t/km^2/a), similar to those observed for the Ogooué River at its mouth, characterize the northern catchments and the Mbei tributaries.

4 Results

Sample name	Production	Difference Quartz	Denudation	Uncertainty	Denudation	Uncertainty	Integration time
	at/g/a	%	m/Ma		t/km2/a		ka
OG-01	3.10	1.50	23.0	1.9	62.1	5.0	26
OG-02	2.92	0	5.8	0.5	15.6	1.2	104

OG-03	3.54	-0.19	6.7	0.5	18.1	1.3	89
OG-04	3.57	0.04	8.7	0.7	23.4	1.7	69
OG-05	3.11	0.05	14.6	1.2	39.3	3.1	41
OG-07	3.14	-0.15	8.3	0.7	22.3	1.7	73
OG-08	3.16	0.07	15.0	1.2	40.4	3.2	40
OG-10	3.12	-0.04	6.4	0.5	17.2	1.3	94
OG-11	3.30	0	4.9	0.4	13.2	1.0	122
OG-12	3.23	0.01	5.1	0.4	13.9	1.0	117
OG-13	3.30	0.06	3.1	0.2	8.3	0.6	196
OG-14	3.07	0	13.4	1.1	36.3	2.9	45
OG-15	3.27	0	6.9	0.5	18.5	1.4	87
OG-16	3.23	0	21.8	1.8	58.9	4.7	28
OG-17	3.37	-0.10	7.0	0.5	18.9	1.4	86
OG-19	3.44	-0.15	18.1	1.4	48.9	3.7	33
OG-20	3.16	0.09	17.3	1.4	46.8	3.6	35
OG-21	3.27	0.04	18.8	1.5	50.8	3.9	32
OG-22	3.27	0.04	11.0	0.9	29.7	2.3	55
OG-24	3.17	0.02	13.8	1.1	37.4	2.9	43
OG-25	2.79	0	7.9	0.6	21.3	1.7	76
OG-26	3.19	0.08	17.6	1.4	47.6	3.7	34
BTK08-5	3.27	0	11.1	0.9	29.9	2.3	54
BTK08-20	3.63	0	19.8	1.5	53.3	3.8	30
BTK08-22	3.37	0	7.3	0.6	19.8	1.5	82

279

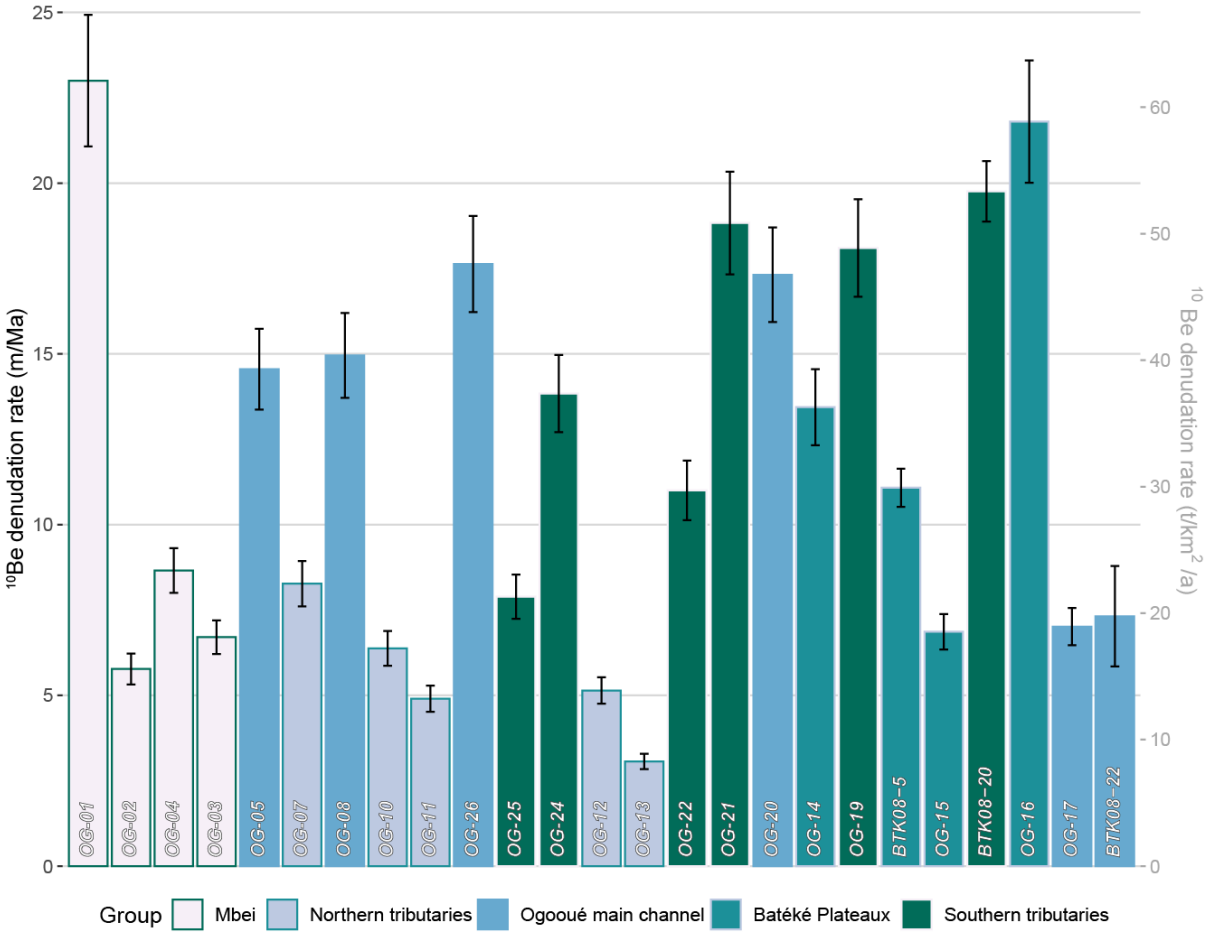

Figure 5. The ^{10}Be-derived denudation rates, ordered from downstream to upstream along the Ogooué main channel. The Mbei rivers (samples# 1 to 4) do not drain to the Ogooué River. [Printed in Black & White]

The ^{10}Be concentrations of the Ogooué sediments show an average catchment denudation rate of approximately 15 m/Ma (~40 t/km^2/a, Figure 5). We obtained these values for the two most downstream samples (OG-5 and OG-8), which integrate most of the catchment area (~200,000 km^2). Following Moquet et al. (2021), we divide the samples into five groups following geomorphological and lithological units (Table 2, Figure 1): the Mbei tributaries (outside of the Ogooué catchment itself), the northern Ogooué tributaries, the Batéké Plateaux tributaries, the southern Ogooué tributaries, and the Ogooué River main channel.

The two most downstream samples (OG-5 and OG-8) integrate most of the catchment area (~200,000 km^2) and provide the average catchment denudation rate. Along the Ogooué main channel, upstream

293 from the lowermost sample (samples OG-5, OG-8, OG-26, OG-20, OG-17 and BTK08-22 in the upstream
294 direction), the evolution of ^{10}Be concentration is not monotonous, with lower concentrations for
295 samples OG-26 and OG-20; this results in higher denudation rates of ~17 m/Ma, 47 t/km^2/a. In
296 comparison, the most upstream Ogooué mainstream sampling site (samples OG-17 and BTK08-22,)
297 displays a higher ^{10}Be concentration, implying a lower denudation rate of 7 m/Ma or 18 t/km^2/ a (Table
298 3 and Figures 5 and 6). The rivers draining the Batéké Plateaux represent the main contributors to the
299 Ogooué between sampling points OG-17 and OG-20.
300 The denudation rates in the Batéké Plateaux area (samples OG-14, OG-15, OG-16, and BTK08-5) are
301 variable, ranging from 7 to 22 m/Ma (18 to 57 t/km^2/a). The denudation rates of the northern
302 tributaries (3-7 m/Ma or 8-19 t/km^2/a) are roughly one or two times lower than those of the southern
303 tributaries (8-20 m/Ma or 21-53 t/km^2/a). The trend in the catchment-scale denudation rate observed
304 along the course of the Ogooué River mainstream (Figure 5) most likely results from the contribution
305 of these tributaries.
306 The position of two samples draining the Batéké Plateaux (BTK08-5 and BTK08-22) in a “banana plot”
307 (^{26}Al/^{10}Be *vs.* ^{10}Be; Figure S1) indicates that these samples are partly made up of recycled material.
308 However, the proximity of the data to the “surface banana” (in black on Figure S1) suggests that the
309 contribution of this recycled material is low, resulting in an underestimate of the ^{10}Be-derived
310 denudation rate by 25% at most.
311

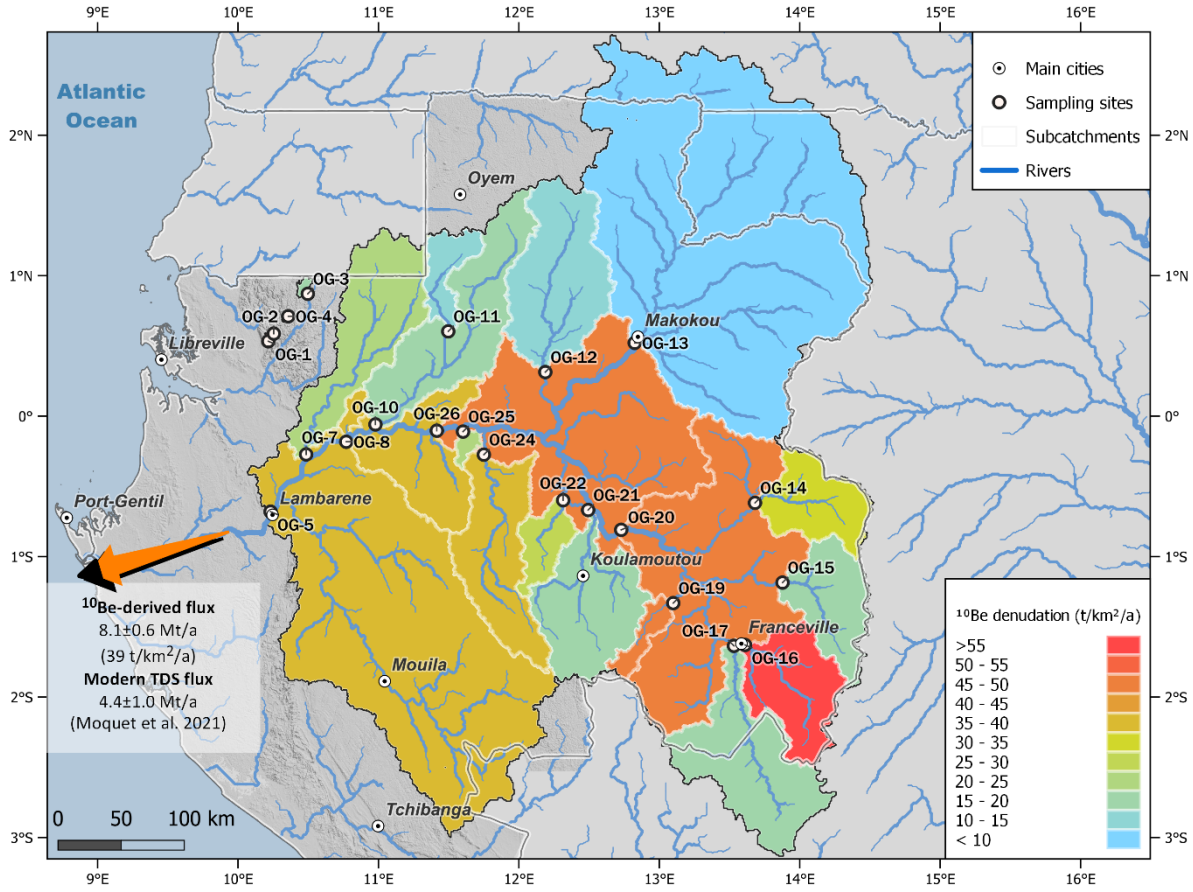

Figure 6. Colored scale map of the ^{10}Be-derived catchment-scale denudation rates for the ORB. The sampling points that define the outlets of the catchment areas are shown as black circles. The modern TDS flux has been evaluated by Moquet et al. (2021) [Printed in Black & White]

The spatial distribution of the denudation rates in the Ogooué catchment can be refined using a "nested catchment approach", where the difference in sediment flux (calculated as the erosion rate x the contributing area) between two stations along the same river provides an estimate of the sediment flux and the erosion rates of the area contributing to the river between these two stations. Despite significant uncertainties (see Supplementary Material Figure S2), these estimates: 1) result in values similar to those stemming from direct ^{10}Be measurements for samples OG-5 and OG-10 (Figure 5), and 2) suggest an erosion that is faster than 80 t/km^2/a for the two nested catchments (OG-20 and OG-26). However, because of the significant uncertainties associated with these estimates, we do not include these numbers in the analysis presented in section 4.2.

We evaluated the interannual variability in the ^{10}Be-derived erosion rate using pairs of samples collected at the same location in 2008 and in 2017. Samples OG-17 and BTK08-22, from the upstream part of the main Ogooué channel, result in similar erosion rates within uncertainty, whereas the ^{10}Be-derived erosion rate from samples OG-15 and BTK08-05, from the Batéké Plateaux, differ by 25%. This difference could come from the variable contribution from the sub-catchments to the sand collected at the sampling sites, and indicates that in addition to analytical uncertainties, long-term estimates of the erosion rates of large, lithologically-mixed catchments of the ORB are affected by other sources of uncertainties, that we estimate to be on the order of 25%.

4.1 ^{10}Be denudation rates *vs.* catchment physical properties

Table 4 summarizes the catchment-scale physical and geomorphological parameters and denudation flux from this work and the chemical denudation rates from Moquet et al. (2021). As commonly observed, the denudation rates increase with the slope, even for low slopes such as those prevailing in the ORB (Figure 7a). The two points that deviate from this relationship are two catchments of the Mbei tributaries, which are most likely too small to be accurately represented by the DEM. The denudation rates do not vary significantly with rainfall (which is relatively invariant across the study area; Figure 7b), catchment elevation (Figure 7c), or river discharge (Figure 7d), as also emphasized by the correlation matrix (Figure 8). In addition, Figure 7e shows that the ^{10}Be integration time decreases with the catchment size, except for the northern tributaries. Conversely, the denudation rates increase with the size of the catchment, except for the northern tributaries.

Table 3. Modern dissolved fluxes († refers to data from Moquet et al., 2021) vs. millennial fluxes. The fluxes are organized by group; the second part of the table indicates group averages and the third one (lowermost) shows the fluxes evaluated by the nested catchment method (see the text and Supplementary Material S2). The catchment properties, Total Dissolved Solids (TDS), results from the ^{10}Be concentrations (denudation rate and fluxes), and integration time are displayed from left to right).

Group	Sample number	Basin area†	Basin average slope†	Basin average elevation†	River annual mean discharge†	Basin average rainfall†	Specific discharge (runoff)†	Modern TDS flux†	Modern TDS flux†	Millenial area-normalized fluxes (^{10}Be)				
										Denudation	Denudation uncertainty	Flux	Flux uncertainty	Integration time
		km²	%	m.a.s.l.	$m^3 s^{-1}$	mm a^1	mm a^{-1}	10^3 t a^{-1}	t km^{-2} a^{-1}	t km^{-2} a^{-1}		10^3 t a^{-1}		10^3 a
Mbei tributaries	1	13	7.9	448	0.29	2244	692	0.24	18	62.1	5.0	0.8	0.1	26
	2	5	7.5	387	0.11	2244	692	0.09	17.2	15.6	1.2	0.1	0.0	104
	3	135	1	639	2.6	1957	604	1.86	13.8	18.1	1.3	2.4	0.2	89
	4	13	0.8	613	0.29	2244	692	0.21	15.8	23.4	1.7	0.3	0.0	69
Ogooué main channel	18 & 08-22	8778	0.7	582	229	2663	821	158	18	19.8	1.5	173.4	12.7	82
	17	14944	1	555	390	2672	824	276	18.5	18.9	1.4	282.9	21.2	86
	20	45823	1.1	493	1126	2512	775	705	15.4	46.8	3.6	2142.5	165.2	35
	26	142373	0.9	502	3044	2186	674	2764	19.4	47.6	3.7	6778.3	520.8	34
	8	160312	1	497	3378	2155	664	3007	18.8	40.4	3.2	6473.2	517.7	40
	5 & 6	205585	1.2	467	**4341***	2159	666	4071	19.8	39.3	3.1	8077.5	632.9	41
Northern Ogooué tributaries	7	8265	1.3	448	155	1915	590	177.8	21.5	22.3	1.7	184.5	14.2	73
	9	483	3	281	9	1933	596	9.7	20.1					
	10	11135	1.1	494	207	1902	587	200	18	17.2	1.3	191.6	14.8	94
	11	2049	0.8	590	39	1935	597	27.2	13.3	13.2	1.0	27.1	2.0	122
	12	8803	0.5	523	169	1967	607	174.5	19.8	13.9	1.0	122.2	8.9	117
	13	49503	0.6	549	949	1960	604	560.9	11.3	8.3	0.6	409.4	29.1	196
Southern Ogooué tributaries	19	1161	1.5	592	29	2579	795	52.7	45.4	48.9	3.7	56.7	4.3	33
	21	7582	1.6	531	176	2368	730	399.6	52.7	50.8	3.9	385.5	29.7	32
	22	2020	1.3	394	44	2236	690	100	49.5	29.7	2.3	60.0	4.6	55
	23 & 24	7057	1.8	493	145	2103	649	240.2	34	37.4	2.9	263.7	20.7	43
	25	379	2	322	7	1890	583	11.9	31.4	21.3	1.7	8.1	0.6	76
Plateaux Batéké	14	4513	0.8	458	101	2287	705	54.6	12.1	36.3	2.9	163.7	13.0	45
	15	4911	1.4	537	129	2692	830	42.8	8.7	18.5	1.4	91.0	6.6	87
	16	5892	1.6	524	155	2682	827	48	8.2	58.9	4.7	346.8	27.5	28
Ogooué catchment average	at Lambaréné	205585	1.2	467	4341*	2159	666	4071	19.8	39.3	3.1	8077.5	632.9	41
Northern Ogooué tributaries	sum/average	80238	0.8	528	1528	1947	3581	1150	14.3	11.7	0.9	934.9	69.0	133
Southern Ogooué tributaries	sum/average	18199	1.6	501	401	2254	678	804	44.2	42.5	3.3	774.0	59.9	37
Plateaux Batéké	sum/average	15317	1.3	509	385	2569	792	145	9.5	39.3	3.1	601.6	47.2	40
Remaining area	sum/average	46558					721	907	11.5	62.5	17.4	5767.0	808.9	
Mbei tributaries	sum/average	166	1.7	614	3.3	2011	620	2.4	14.5	21.9	9.2	3.6	0.3	71
Nested	20n	14402	1.0	404		2280		230.9	16.0	83.4	16.5	1201.3	237.9	
Nested	26n	21206	0.7	409		2063		571.9	27.0	159.7	36.8	3386.9	779.6	
Nested	8n	6804	2.9	397		1920		43	6.3	-73.0	154.8	-496.7	1053.3	
Nested	5n	37008	2.0	341		2231		886.2	23.9	38.4	31.5	1419.8	1164.8	
Nested	10n	9086	1.2	472		1895		172.8	19.0	18.1	1.8	164.5	16.8	

349

350

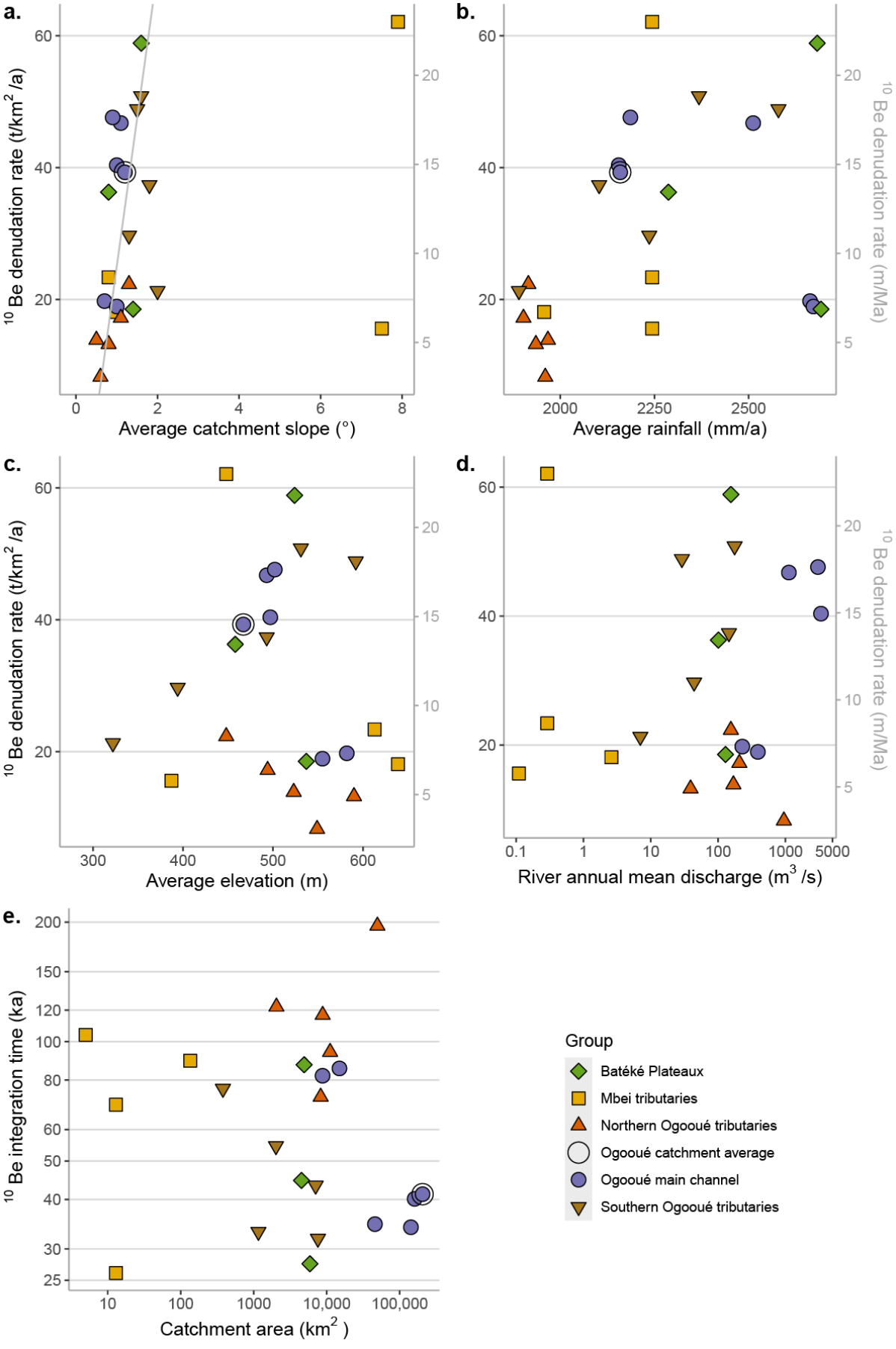
a.
b.
c.
d.
e.
^{10}Be denudation rate (t/km^2 /a)
^{10}Be denudation rate (m/Ma)
Average catchment slope (°)
Average rainfall (mm/a)
Average elevation (m)
River annual mean discharge (m^3 /s)
^{10}Be integration time (ka)
Catchment area (km^2)
Group
Batéké Plateaux
Mbei tributaries
Northern Ogooué tributaries
Ogooué catchment average
Ogooué main channel
Southern Ogooué tributaries

351

Figure 7. a. Catchment-scale ^{10}Be denudation rate vs. catchment average slope. b. Catchment-scale ^{10}Be denudation rate vs. catchment average rainfall. c. Catchment-scale ^{10}Be denudation rate vs. catchment average elevation, d. Catchment-scale ^{10}Be denudation rate vs. river discharge. e. ^{10}Be integration time vs. catchment area (in log scale). Note that the integration times are, by definition, inversely proportional to the ^{10}Be denudation rates. [Printed in Black & White]

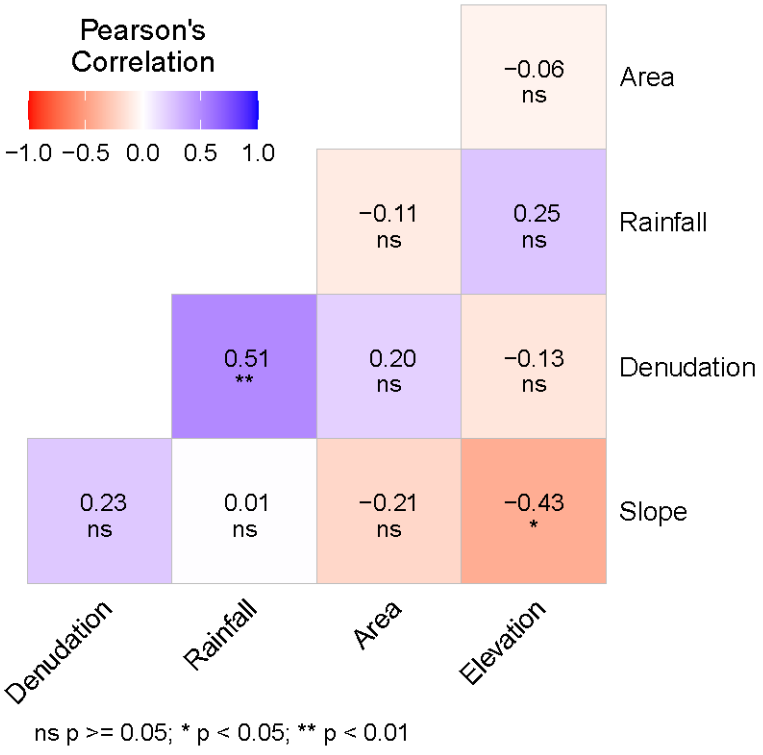

Figure 8. Pearson correlation matrix between the catchment-scale ^{10}Be denudation rate ("Denudation"), catchment area, catchment average rainfall, catchment average slope and catchment average denudation. "ns": not significant; we note that most of the correlations are not significant.

4.2 ^{10}Be millennial denudation rates *vs.* modern denudation

Figure 9 represents our millennial cosmogenic ^{10}Be flux *vs.* the modern TDS specific flux (Table 4). It is important to note that these two methods differ both in terms of the types of processes they account for (physical + part of chemical for ^{10}Be *vs*. chemical for solute fluxes) and the time scale over which they integrate these processes (millennial for ^{10}Be *vs*. several years for solute fluxes). Assuming that the determined modern chemical denudation rates have prevailed over the last two hundred thousand years (maximum ^{10}Be integration time), the 1:1 line drawn in Figure 9 corresponds to sites where denudation is only chemical (congruent dissolution, no transport), whereas the 2:1 line delineates the

case of equal contributions from chemical and physical denudation. However, in this tropical cratonic type of environment, the regolith is often thick (>> 1m), and the ^{10}Be measurements do not record the chemical denudation that is mostly taking place at the weathering front, i.e. at the base of the regolith. Thus, in the ORB, ^{10}Be probably only reflects physical erosion and therefore the 1:1 line would represent locations with equal rates of chemical and physical denudation and the 2:1 line would indicate locations where chemical denudation accounts for ⅓ of the total denudation (⅔ of the physical denudation). As congruent rock dissolution is rare (since it would require releasing elements that are insoluble such Al and Fe into a solution), data points lying on or below the 1:1 line can only be explained if the ^{10}Be measurement cannot record anything about the weathering, as it occurs too deeply below the ^{10}Be production zone and/or chemical weathering has recently increased and/or analytical issues have arisen.

In addition, in Figure 9, the points may be shifted either to the right in the areas that underwent a recent increase in the chemical denudation rates (area below the 1:1 line) or to the left in areas that underwent a recent decrease (area above the 2:1 line). This is the case for the southern Ogooué tributaries, as two of them display points below the 1:1 line (sample points OG-22 and OG-25; the latter corresponds to the smallest documented catchment excluding the Mbei tributaries).

In Figure 9, data from the southern and northern tributaries of the Ogooué as well as from the Mbei tributaries, plot close to the 1:1 line, suggesting that chemical denudation represents a significant part of the total denudation in these regions (i.e. the chemical denudation is of the same order of magnitude as the physical erosion). Conversely, the Batéké Plateaux area is characterized by a lower contribution of chemical weathering processes to the total denudation.

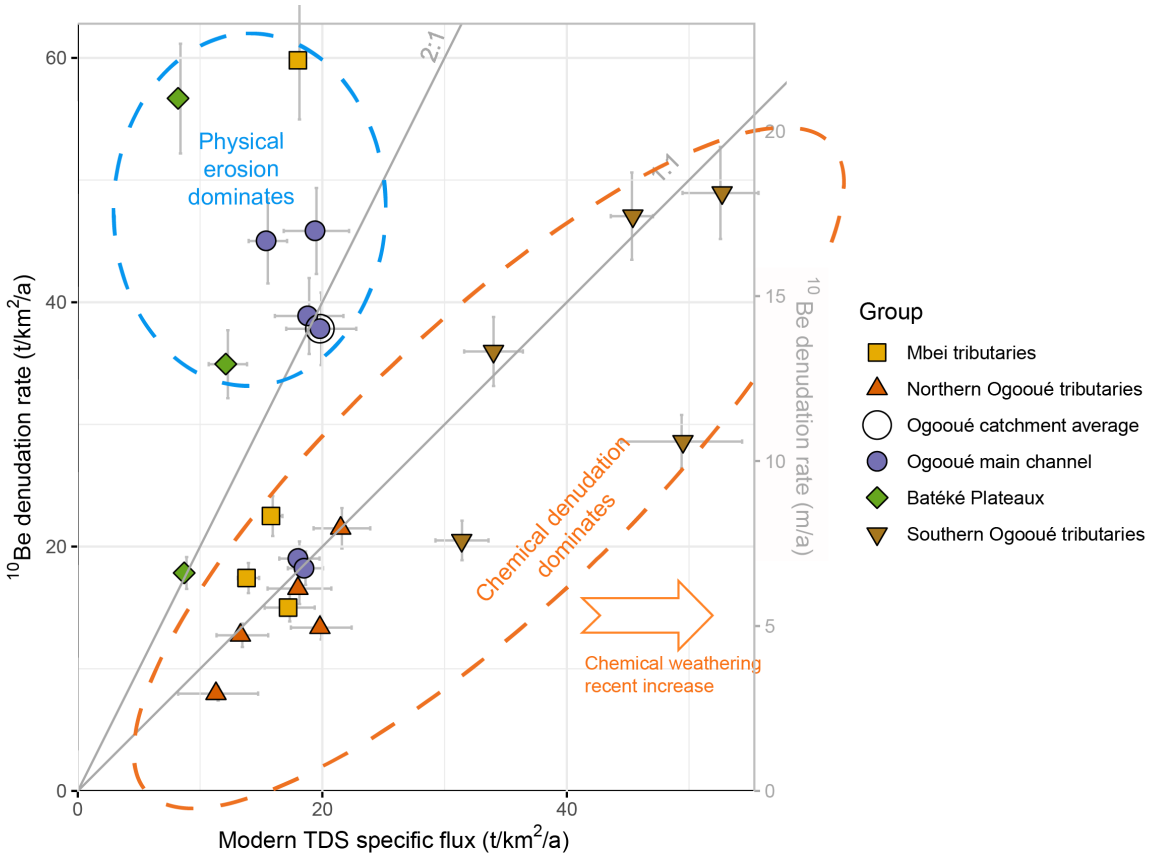

Figure 9. Millennial ^{10}Be denudation rate vs modern TDS specific flux (from Moquet et al. 2021). Horizontal and vertical bars indicate uncertainties. The orange ellipse delineates a group of points lying close to the 1:1 line, corresponding to catchments where chemical denudation is dominant. The blue ellipse indicates catchments where denudation occurs mainly as physical denudation while the orange ellipse indicates catchments where denudation occurs mainly as chemical weathering.Given that the two approaches yield fluxes averaged over different characteristic times, a recent increase in chemical denudation should shift the points to the right, indicated by the arrow (see text). [Printed in Black & White]

5 Discussion

5.1 Distribution of denudation rates within the Ogooué catchment

Our data confirm that the Ogooué catchment can be subdivided into distinct sub-areas (Figures 4 to 7). In particular, most sub-catchments show that chemical denudation significantly contributes (> ⅓) to the total denudation, as observed in many similar cratonic areas (Figure 9). An exception to this general behavior includes the river draining the Batéké Plateaux and one Mbei tributary (OG-01). The

Batéké Plateaux are characterised by high physical erosion rates and low chemical denudation rates (Figure 9). The northern Ogooué catchments are characterized by: 1) a decrease in the denudation rate with catchment area (Figure 7e), 2) slopes and denudation rates well below the ORB average (Figure 7a), and 3) ^{10}Be denudation rates similar to the chemical denudation rates (Figure 9). The southern tributaries display high denudation rates along with a significant chemical contribution (Figure 9). In the following, each of these sub-units is discussed separately.

5.1.1 Batéké Plateaux

The Batéké Plateaux area in the south-eastern part of the Ogooué catchment are underlain by mostly quartzitic aeolian unconsolidated Cenozoic sands with local sandstones (Séranne et al., 2008; Thiéblemont et al., 2009a) and are characterized by relatively high denudation rates (20-60 t/km^2/a or 7-22 m/Ma) with a small contribution of chemical denudation (< 15 t/km^2/a, Figure 9). This prominent role of physical processes in the denudation of this region reflects the combination of two characteristics: (i) the initial material (quartzitic aeolian sands) corresponds to the product of ancient alteration episodes and is no longer prone to weathering (except for the alteration of disseminated oxides, which gives the sands their pink to red color, Figure 10); and (ii) the material is mainly unconsolidated and susceptible to mechanical erosion. This interpretation is confirmed by field observations of active erosion and incision in sandy formations with little cohesion. In particular, regressive erosion forms were observed during our field campaigns, resulting in “badland-like” morphologies, with steaphead valleys called “cirques” filled with reworked sand (Figure 10). The escarpments delineating these valleys locally display slopes > 45° at the level of the bordering crests.

Figure 10. View of a "cirque" in the Batéké Plateaux. This landform is similar to the lavakas in Madagascar. [Printed in Black & White]

5.1.2 Northern tributaries

The catchments of the northern tributaries are characterized by shallow slopes and a low denudation rate, the magnitude of which is close to chemical denudation (8-22 t/km2/a; Figure 9). The whole area forms a plateau in continuity with the south of Cameroon, where low erosion and chemical denudation rates are also observed (Regard et al., 2016). These observations could indicate either a dominance of chemical processes on the total denudation, and/or a recent increase in the chemical denudation rates. The relief of the area drained by the northern tributaries is relatively flat, with not much variation in rock type, which may explain the low denudation rates and the high contribution of the chemical denudation.

5.1.3 Southern tributaries

The southern tributaries show a relatively high rate of erosion, of the same order of magnitude as the Batéké Plateaux. However, unlike in the Batéké Plateaux, erosion in the southern ORB is associated with significant chemical denudation (Figure 9). Indeed, the basement of the southern tributaries

mainly consists of granitoids (Chaillu Massif) and Francevillian sedimentary rocks (mainly sandstones and shales) prone to chemical weathering (abundant feldspars). The relief is indeed more marked than in the north (except for greenstone belts) which could favor both physical erosion and weathering (D. Thiéblemont, pers comm).

5.1.4 Mbei tributaries

The Mbei tributaries correspond to small catchments outside of the Ogooué Basin but which drain similar lithologies. Two of the corresponding samples (OG-03 and OG-04) drain a plateau area with low average slopes, whereas two other samples (OG-01 and OG-02) were collected in rivers draining the edge of the Mbei catchment, which is characterized by higher slopes. Across these samples, the denudation is low (14-22 t/km^2/a or 5-9 m/Ma), and the ratio between the ^{10}Be-derived erosion rates and solute-flux derived chemical denudation is between 1 and 2, with the notable exception of OG-01 (Figure 9). Except for OG-01, these catchments behave similarly to the northern Ogooué tributaries, with either a dominance of chemical processes on total denudation, and/or a recent increase in the chemical denudation rates. However, the Mbei tributaries lie slightly closer to the 2:1 line in Figure 9 than the other Ogooué tributaries do, perhaps reflecting the proximity of the plateau edge where a recent increase in denudation is likely.

5.1.5 Ogooué mainstream

Apart from the two most upstream points where low denudation rates are recorded, no significant change in denudation is observed along the Ogooué mainstream (around 15 m/Ma or 40 t/km^2/a). The erosion rates estimated through the “nested catchment approach” suggest a fast denudation of the river alluvial plain (~100 t/km^2/a), although these estimates are associated with strong uncertainties.

5.1.6 Summary of the denudation spatial distribution

To summarize, the northern Ogooué sub-catchments are eroding more slowly than the southern counterparts, including those draining the Batéké Plateaux. At first sight, this difference can be explained by the (slightly) steeper slopes in the south (Figure 7a). These steeper slopes are not due to

differences in elevation (Figure 7c), but instead reflect a more incised topography and a more pronounced relief (see Figure 1). Another explanation is that the higher denudation rates could reflect a transient adjustment over long timescales, as proposed by Vanacker et al. (2007) to explain the difference in Sri Lanka between low denudation rate areas for large river systems in the coastal plains (~5 m/Ma), and high denudation rates in the highlands (~45 m/Ma). This latitudinal distinction among the Ogooué sub-catchments was already noted by Moquet et al. (2021) based on the hydrochemistry and solute fluxes. Moquet et al. (2021) proposed that this difference in terms of chemical weathering rates could be caused by uplift in the southern region, potentially related to a mantle-induced dynamic uplift or lithospheric processes affecting the rims of the Congo Cuvette located to the south of the Ogooué catchment. We are therefore now able to view this latitudinal difference in terms of the total denudation rates, which are on the order of 40 t/km^2/a (15 m/Ma) across the southern part of the Ogooué catchment (including the Batéké Plateaux), and less than half (~15 t/km^2/a or 6 m/Ma) in the northern part of the study area (including the Mbei catchment).

Within this pattern, there is no influence of integration time scales which, in any case, are always longer than the age of the last glaciation, and sometimes up to almost 200 ka. As observed elsewhere (e.g. Regard et al., 2016), there does not seem to be any noticeable evolution in the processes at a time scale of the Quaternary glacial climate cycles.

5.2 Low denudation rates at the scale of the whole Ogooué catchment

The contribution of the Ogooué River to the total West African Equatorial (Atlantic coast from Senegal to Angola) discharge is ~7% (Moquet et al., 2021) for a contributory surface area of 2.6%. In comparison, the solute flux of the Ogooué River, 4.1 Mt/yr, is 5% of the total solute flux of West Africa (Milliman and Farnsworth, 2011; Moquet et al., 2021). The millennial-scale denudation flux is 8.1 Mt/a (38 t/km^2/a), including physical erosion and part of the TDS (see section 4.3) at the West African scale, and corresponding to 4 to 6% of the total denudation flux (TSS + TDS ~220 Mt/a and TSS ~130 Mt/a only, evaluated over the same area as in Milliman and Farnsworth, 2011). Therefore, although the Ogooué catchment is characterized by a low rate of weathering compared to the global average, this

rate is higher than the West African Equatorial average (21 *vs.* 11 t/km^2/a). Similarly, the millennial-scale total denudation rate is low (15 m/Ma) and is characteristic of stable cratonic areas (e.g. Beauvais and Chardon, 2013; Regard et al., 2016), but is slightly higher than the corresponding West African Equatorial average (38 *vs*. 26 t/km^2/a).

To compare our Ogooué data with other settings worldwide, Figure 11 shows a compilation of the ^{10}Be-derived denudation rates measured in cratonic areas plotted against the corresponding solute fluxes representing the rate of chemical weathering. The Ogooué data are close to the 1:1 line, meaning that the chemical to total denudation ratio is high in this catchment. This prevalence of chemical processes on the total denudation is relatively rare among cratonic catchments, even when considering tropical catchments only (Figure 11). Consequently, our study area stands out as a very stable cratonic setting, in which denudation is largely due to chemical weathering (see section 4.3). In particular, it is characterized by a thick regolith, which often occurs concurrently with relative equivalence between chemical weathering and physical denudation (Braun et al., 2012).

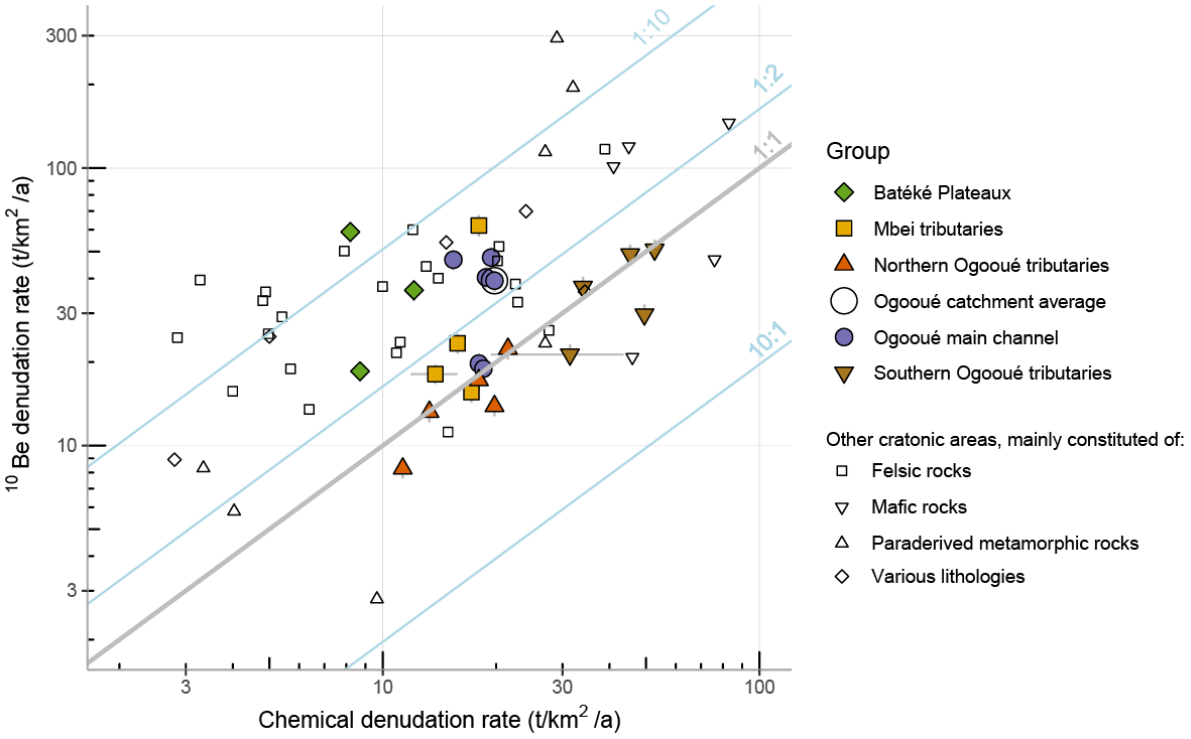

Figure 11. Millennial ^{10}Be-derived denudation rates vs. modern solute specific flux (in logarithmic scale) for ORB and other rivers draining cratonic areas worldwide: Oubangi, Congo, Niger, Zambesi, Fish, Molopo, Orange, Okavango, Limpopo, Murray and Darling, Finke, Macumba, Neales, St. Lawrence, Mississippi, Volga, Dniepr, Lena (Wittmann et al., 2020); Mpanga North, Dunga, Igasa, Ruimi, Mobuku, Isebo, Kilembe, Mpanga South, Dura (Hinderer et al., 2013); Maracuja, Caraca (Salgado et al., 2007); Cristiano Otoni, Sao Geraldo (Cherem et al., 2012b, 2012a); Selenga, Turka, Barguzin, Upper Angara, Kichera (Suhrhoff et al., 2022); Nyong, Mengong, Bivesse, Awout, Soo, Mbam, Sanaga (Regard et al., 2016), Branco and Tapajos (Filizola and Guyot, 2009; Wittmann et al., 2011). The lithology indicated in the legend has been evaluated from the original publications and from the GLiM databse (Hartmann and Moosdorf, 2012). The lines show the particular ratios between the chemical denudation and ^{10}Be denudation rates; the 1:1 line depicts the equivalent denudation rates. [Printed in Black & White]

5.3 Is denudation in the Ogooué landscape operating at equilibrium?

In this work, we combine the estimates of the denudation rates based on solute fluxes and the ^{10}Be measurements. Solute fluxes provide information on modern (i.e. typically integrated over several years) chemical denudation, whereas ^{10}Be essentially provides information on longer-term physical denudation (25 to 200 ka, see Table 4), possibly encompassing a chemical denudation component for areas where the regolith is thin (< 1m). This combination allows us to address the equilibrium status of the landscape of the study area. Denudation at equilibrium is achieved if the nature and thickness

of the regolith do not change over time (e.g. Heimsath et al., 1997). This condition is more or less equivalent to the rate of downward progression of the weathering front being the same as the rate of lowering of the Earth's surface by denudation. A rigorous test of this hypothesis requires knowledge of the proportion of the rock material that is lost by dissolution at the weathering front versus what is lost upwards within the regolith. This apportionment is typically made accessible through the quantification of the depletion of soluble elements along weathering profiles (Dixon et al., 2009; Regard et al., 2016; Riebe et al., 2003; Riebe and Granger, 2013), a constraint that is not available at the moment. In addition, it would ideally be necessary to verify that modern physical denudation rates (obtained through sediment gauging) are comparable to those quantified over longer time scales based on ^{10}Be concentrations.

However, in the case of the ORB and with the available data, we can assume that 1) the regolith is generally thick enough for the ^{10}Be fluxes to only measure the physical denudation and 2) the ^{10}Be-derived erosion rates are representative of modern physical erosion. Under such an assumption, equilibrium denudation means that points plotting along the 1:1 line in Figures 9 and 11 describe landscapes where the physical denudation rate is equivalent to the chemical denudation rate. This condition is similar to what has been observed in two soil pits in southern Cameroon, immediately north of the study area (Braun et al., 1998; Regard et al., 2016). We conclude that the landscape is either at or close to equilibrium (note that we exclude the Batéké Plateaux region from this analysis, as the loss in solute there occurred during ancient weathering episodes – not necessarily in situ). In this case, the contrasted denudation rate between the northern and southern Ogooué tributaries suggests that weathering rates across the Ogooué catchments are "supply-limited", i.e. limited by physical erosion rates (e.g. Riebe et al., 2017).

6 Conclusion

The ^{10}Be measurements provide information on the long-term denudation rate of the Ogooué River catchment. The temporal range is indicated by the integration time, ranging from 25 ka in the fastest

denuding parts (e.g. OG-16) to 200 ka (OG-13). The integration time averaged over the entire catchment is 40 ka. The Ogooué River catchment denudes at a relatively slow rate (38 t/km^2/a, 15 m/Ma), slightly higher than the West African average (~26 t/km^2/a, ~10 m/Ma, evaluated from Milliman and Farnsworth, 2011). Physical denudation and chemical weathering are of the same order of magnitude. This shows that, although low, there is substantial chemical weathering compared to physical denudation, with a contribution that is likely >30% of the total denudation.

However, this large-scale observation is associated with denudation rates that are spatially variable (10-60 t/km^2/a). This variability exhibits a fairly close balance of physical denudation/chemical weathering over the long term (close to the 1:1 line on Figure 11). Noticeably, there is an overall strong correlation between the chemical denudation rates and physical erosion rates. This supports the scenario of supply-limited weathering, where chemical denudation contributes to a large part of the total denudation. The data points from the Batéké Plateaux are outside this trend, because they are made up of detrital material that has already been weathered and therefore they have a very low modern flux of solutes. The results of this study confirm and complement the work of Moquet et al. (2021), i.e. the southern part of the catchment is denuding twice as fast as the northern part, and that denudation over the whole catchment has not varied much since 100 ka, as shown by both methods which give consistent results. Higher denudation rates to the south could be caused by uplift (Guillocheau et al., 2018). Uplift in the area may operate over a long wavelengths (> 1000 km), spanning a time scale of millions of years, and could be due to deep-seated mantle upwelling (e.g. Cottrell et al., 2004; Guillocheau et al., 2018; Hu et al., 2018).

Funding

This study was supported by the RALTERAC EC2CO INSU project, the International Joint Laboratory DYCOFAC (Dynamics of the forested ecosystems of Central Africa in a context of global change) and the Programme Emergences of the City of Paris “Chemical weathering of sediments in large tropical floodplains” (agreement 205DDEEES165). The ^{10}Be and ^{26}Al analyses were performed at the ASTER

AMS national facility (CEREGE, Aix-en-Provence), and were supported by the INSU/CNRS, the ANR through the “Projets thématiques d'excellence” program for the “Equipements d'excellence” ASTER-CEREGE action, and the Institut de Recherche pour le Développement (IRD).

Acknowledgements

We would especially like to thank Dr. Aurélie Flore Koumba Pambo for the research authorizations in Gabon, Jean-Grégoire Kayoum for driving and taking photographs during the sampling field campaign, and D. Thiéblemont (BRGM) for constructive discussions about the geology of the Ogooué catchment. We would also like to thank the ANPN and CIRMF for their support during the field campaign. This work is a contribution of the dating facility at GET in Toulouse, and we are very grateful for the strong support from the GET lab. Verle Vanacker, Denis Thiéblemont and Jan Marten Huizenga are acknowledged for their fruitful comments.

Author contributions

Conceptualization: JJB, JSM, VR, SCa, JB; funding acquisition: JJB, JB, VR; field work: JSM, JJB, SB, MS and APM; cosmogenic nuclide measurements and data analysis: VR, SCa, SCh, PHN, JC; writing-original draft: VR, SCa & JSM; writing-review and editing: all authors.

References

Al-Hajri, Y., White, N., Fishwick, S., 2009. Scales of transient convective support beneath Africa. Geology 37, 883–886. https://doi.org/10.1130/G25703A.1

Arnold, M., Merchel, S., Bourlès, D.L., Braucher, R., Benedetti, L., Finkel, R.C., Aumaître, G., Gottdang, A., Klein, M., 2010. The French accelerator mass spectrometry facility ASTER: Improved performance and developments. Nucl. Instrum. Methods Phys. Res. Sect. B Beam Interact. Mater. At., 19th International Conference on Ion Beam Analysis 268, 1954–1959. https://doi.org/10.1016/j.nimb.2010.02.107

Balco, G., Stone, J.O., Lifton, N.A., Dunai, T.J., 2008. A complete and easily accessible means of calculating surface exposure ages or erosion rates from Be-10 and Al-26 measurements. Quat. Geochronol. 3, 174–195.

Beauvais, A., Chardon, D., 2013. Modes, tempo, and spatial variability of Cenozoic cratonic denudation: The West African example. Geochem. Geophys. Geosystems 14, 1590–1608. https://doi.org/10.1002/ggge.20093

Bogning, S., Frappart, F., Blarel, F., Nino, F., Mahé, G., Bricquet, J.-P., Seyler, F., Onguéné, R., Etame, J., Paiz, M.-C., 2018. Monitoring water levels and discharges using radar altimetry in an ungauged river basin: The case of the Ogooué. Remote Sens. 10, 350.

Braucher, R., Guillou, V., Bourlès, D.L., Arnold, M., Aumaître, G., Keddadouche, K., Nottoli, E., 2015. Preparation of ASTER in-house 10Be/9Be standard solutions. Nucl. Instrum. Methods Phys. Res. Sect. B Beam Interact. Mater. At., The Thirteenth Accelerator Mass Spectrometry Conference 361, 335–340. https://doi.org/10.1016/j.nimb.2015.06.012

Braucher, R., Merchel, S., Borgomano, J., BourlÃ¨s, D.L., 2011. Production of cosmogenic radionuclides at great depth: A multi element approach. Earth Planet. Sci. Lett. 309, 1–9. https://doi.org/10.1016/j.epsl.2011.06.036

Braun, J.-J., Marechal, J.-C., Riotte, J., Boeglin, J.-L., Bedimo Bedimo, J.-P., Ndam Ngoupayou, J.R., Nyeck, B., Robain, H., Sekhar, M., Audry, S., Viers, J., 2012. Elemental weathering fluxes and saprolite production rate in a Central African lateritic terrain (Nsimi, South Cameroon). Geochim. Cosmochim. Acta 99, 243–270. https://doi.org/10.1016/j.gca.2012.09.024

Braun, J.-J., Viers, J., Dupré, B., Polve, M., Ndam, J., Muller, J.-P., 1998. Solid/Liquid REE Fractionation in the Lateritic System of Goyoum, East Cameroon: The Implication for the Present Dynamics of the Soil Covers of the Humid Tropical Regions. Geochim. Cosmochim. Acta 62, 273–299. https://doi.org/10.1016/S0016-7037(97)00344-X

Burbank, D.W., Leland, J., Fielding, E., Anderson, R.S., Brozovic, N., Reid, M.R., Duncan, C., 1996. Bedrock incision, rock uplift and threshold hillslopes in the northwestern Himalayas. Nature 379, 505–510. https://doi.org/10.1038/379505a0

Carretier, S., Regard, V., Vassallo, R., Aguilar, G., Martinod, J., Riquelme, R., Pepin, E., Charrier, R., Hérail, G., Farías, M., Guyot, J.-L., Vargas, G., Lagane, C., 2013. Slope and climate variability control of erosion in the Andes of central Chile. Geology 41, 195–198. https://doi.org/10.1130/G33735.1

Charreau, J., Blard, P.-H., Zumaque, J., Martin, L.C.P., Delobel, T., Szafran, L., 2019. Basinga: A cell-by-cell GIS toolbox for computing basin average scaling factors, cosmogenic production rates and denudation rates. Earth Surf. Process. Landf. 44, 2349–2365. https://doi.org/10.1002/esp.4649

Cherem, L.F.S., Varajão, C.A.C., Braucher, R., Bourlés, D., Salgado, A.A.R., Varajão, A.C., 2012a. Long-term evolution of denudational escarpments in southeastern Brazil. Geomorphology 173–174, 118–127. https://doi.org/10.1016/j.geomorph.2012.06.002

Cherem, L.F.S., Varajão, C.A.C., Salgado, A.A.R., Varajão, A.F.D.C., Braucher, R., Bourlés, D., Júnior, A.P.M., Júnior, H.Á.N., 2012b. DENUDAÇÃO QUÍMICA E REBAIXAMENTO DO RELEVO EM BORDAS INTERPLANÁLTICAS COM SUBSTRATO GRANÍTICO: DOIS EXEMPLOS NO SE DE MINAS GERAIS. Rev. Bras. Geomorfol. 13. https://doi.org/10.20502/rbg.v13i1.344

Chmeleff, J., von Blanckenburg, F., Kossert, K., Jakob, D., 2010. Determination of the Be-10 half-life by multicollector ICP-MS and liquid scintillation counting. Nucl. Instrum. Methods Phys. Res. Sect. B-Beam Interact. Mater. At. 268, 192–199.

Codilean, A.T., Munack, H., Cohen, T.J., Saktura, W.M., Gray, A., Mudd, S.M., 2018. OCTOPUS: an open cosmogenic isotope and luminescence database. Earth Syst. Sci. Data 10, 2123–2139. https://doi.org/10.5194/essd-10-2123-2018

Cottrell, E., Jaupart, C., Molnar, P., 2004. Marginal stability of thick continental lithosphere. Geophys. Res. Lett. 31. https://doi.org/10.1029/2004GL020332

DiBiase, R.A., 2018. Short communication: Increasing vertical attenuation length of cosmogenic nuclide production on steep slopes negates topographic shielding corrections for catchment erosion rates. Earth Surf. Dyn. 6, 923–931. https://doi.org/10.5194/esurf-6-923-2018

Dixon, J.L., Heimsath, A.M., Amundson, R., 2009. The critical role of climate and saprolite weathering in landscape evolution. Earth Surf. Process. Landf. 34, 1507–1521. https://doi.org/10.1002/esp.1836

Ferrier, K.L., Kirchner, J.W., 2008. Effects of physical erosion on chemical denudation rates: A numerical modeling study of soil-mantled hillslopes. Earth Planet. Sci. Lett. 272, 591–599. https://doi.org/10.1016/j.epsl.2008.05.024

Filizola, N., Guyot, J.L., 2009. Suspended sediment yields in the Amazon basin: an assessment using the Brazilian national data set. Hydrol. Process. 23, 3207–3215. https://doi.org/10.1002/hyp.7394

Galy, A., France-Lanord, C., 2001. Higher erosion rates in the Himalaya: Geochemical constraints on riverine fluxes. Geology 29, 23–26. https://doi.org/10.1130/0091-7613(2001)029<0023:HERITH>2.0.CO;2

Godard, V., Bourles, D.L., Spinabella, F., Burbank, D.W., Bookhagen, B., Fisher, G.B., Moulin, A., Leanni, L., 2014. Dominance of tectonics over climate in Himalayan denudation. Geology 42, 243–246. https://doi.org/10.1130/G35342.1

Granger, D.E., Riebe, C.S., 2007. Cosmogenic Nuclides in Weathering and Erosion, in: Treatise on Geochemistry, Volume 5: Surface and Ground Water, Weathering, and Soils. Drever, J.I. (Ed), Elsevier, London.

Guillocheau, F., Chelalou, R., Linol, B., Dauteuil, O., Robin, C., Mvondo, F., Callet, Y., Colin, J.-P., 2015. Cenozoic Landscape Evolution in and Around the Congo Basin: Constraints from Sediments and Planation Surfaces, in: Geology and Resource Potential of the Congo Basin (de Wit, M., Guillocheau, F., de WIt M.C.J., Regional Geology Reviews. Springer, pp. 271–313.

Guillocheau, F., Simon, B., Baby, G., Bessin, P., Robin, C., Dauteuil, O., 2018. Planation surfaces as a record of mantle dynamics: The case example of Africa. Gondwana Res., Rifting to Passive Margins 53, 82–98. https://doi.org/10.1016/j.gr.2017.05.015

Hartmann, J., Moosdorf, N., 2012. The new global lithological map database GLiM: A representation of rock properties at the Earth surface. Geochem. Geophys. Geosystems 13. https://doi.org/10.1029/2012GC004370

Heimsath, A.M., Dietrich, W.E., Nishiizumi, K., Finkel, R.C., 1997. The soil production function and landscape equilibrium. Nature 388, 358–361. https://doi.org/10.1038/41056

Hewawasam, T., von Blanckenburg, F., Bouchez, J., Dixon, J.L., Schuessler, J.A., Maekeler, R., 2013. Slow advance of the weathering front during deep, supply-limited saprolite formation in the tropical Highlands of Sri Lanka. Geochim. Cosmochim. Acta 118, 202–230. https://doi.org/10.1016/j.gca.2013.05.006

Hinderer, M., Pflanz, D., Schneider, S., 2013. Chemical Denudation Rates in the Humid Tropics of East Africa and Comparison with 10Be-Derived Erosion Rates. Procedia Earth Planet. Sci., Proceedings of the Fourteenth International Symposium on Water-Rock Interaction, WRI 14 7, 360–364. https://doi.org/10.1016/j.proeps.2013.03.047

Hu, J., Liu, L., Faccenda, M., Zhou, Q., Fischer, K.M., Marshak, S., Lundstrom, C., 2018. Modification of the Western Gondwana craton by plume–lithosphere interaction. Nat. Geosci. 11, 203–210. https://doi.org/10.1038/s41561-018-0064-1

Kittel, C.M., Nielsen, K., Tøttrup, C., Bauer-Gottwein, P., 2018. Informing a hydrological model of the Ogooué with multi-mission remote sensing data. Hydrol. Earth Syst. Sci. 22, 1453–1472.

Korschinek, G., Bergmaier, A., Faestermann, T., Gerstmann, U.C., Knie, K., Rugel, G., Wallner, A., Dillmann, I., Dollinger, G., von Gostomski, Ch.L., 2010. A new value for the half-life of 10Be by Heavy-Ion Elastic Recoil Detection and liquid scintillation counting. Nucl. Instrum. Methods Phys. Res. Sect. B Beam Interact. Mater. At. 268, 187–191. https://doi.org/10.1016/j.nimb.2009.09.020

Kottek, M., Grieser, J., Beck, C., Rudolf, B., Rubel, F., 2006. World Map of the Köppen-Geiger climate classification updated. Meteorol. Z. 15, 259–263. https://doi.org/10.1127/0941-2948/2006/0130

Laraque, A., Bernal, C., Bourrel, L., Darrozes, J., Christophoul, F., Armijos, E., Fraizy, P., Pombosa, R., Guyot, J.L., 2009. Sediment budget of the Napo River, Amazon basin, Ecuador and Peru. Hydrol. Process. 23, 3509–3524.

Larsen, I.J., Montgomery, D.R., Greenberg, H.M., 2014. The contribution of mountains to global denudation. Geology 42, 527–530. https://doi.org/10.1130/G35136.1

Lupker, M., Blard, P.-H., Lavé, J., France-Lanord, C., Leanni, L., Puchol, N., Charreau, J., Bourlès, D., 2012. 10Be-derived Himalayan denudation rates and sediment budgets in the Ganga basin. Earth Planet. Sci. Lett. 333–334, 146–156. https://doi.org/10.1016/j.epsl.2012.04.020

Maffre, P., Ladant, J.-B., Moquet, J.-S., Carretier, S., Labat, D., Goddéris, Y., 2018. Mountain ranges, climate and weathering. Do orogens strengthen or weaken the silicate weathering carbon sink? Earth Planet. Sci. Lett. 493, 174–185. https://doi.org/10.1016/j.epsl.2018.04.034

Martin, L.C.P., Blard, P.-H., Balco, G., Lavé, J., Delunel, R., Lifton, N., Laurent, V., 2017. The CREp program and the ICE-D production rate calibration database: A fully parameterizable and updated online tool to compute cosmic-ray exposure ages. Quat. Geochronol. 38, 25–49. https://doi.org/10.1016/j.quageo.2016.11.006

Milliman, J., Farnsworth, K., 2011. River Discharge to the Coastal Ocean: A Global Synthesis. Cambridge University Press, Cambridge. https://doi.org/10.1017/CBO9780511781247

Moquet, J.-S., Bouchez, J., Braun, J.-J., Bogning, S., Mbonda, A.P., Carretier, S., Regard, V., Bricquet, J.-P., Paiz, M.-C., Mambela, E., Gaillardet, J., 2021. Contrasted Chemical Weathering Rates in Cratonic Basins: The Ogooué and Mbei Rivers, Western Central Africa. Front. Water 2. https://doi.org/10.3389/frwa.2020.589070

Nishiizumi, K., Imamura, M., Caffee, M.W., Southon, J.R., Finkel, R.C., McAninch, J., 2007. Absolute calibration of Be-10 AMS standards. Nucl. Instrum. Methods Phys. Res. Sect. B-Beam Interact. Mater. At. 258, 403–413.

Picouet, C., Dupré, B., Orange, D., Valladon, M., 2002. Major and trace element geochemistry in the upper Niger river (Mali): physical and chemical weathering rates and CO2 consumption. Chem. Geol. 185, 93–124. https://doi.org/10.1016/S0009-2541(01)00398-9

Puchol, N., Charreau, J., Blard, P.-H., Lavé, J., Dominguez, S., Pik, R., Saint-Carlier, D., Team, A., 2017. Limited impact of Quaternary glaciations on denudation rates in Central Asia. Bulletin 129, 479–499.

Regard, V., Carretier, S., Boeglin, J.-L., Ndam Ngoupayou, J.-R., Dzana, J.-G., Bedimo Bedimo, J.-P., Riotte, J., Braun, J.-J., 2016. Denudation rates on cratonic landscapes: comparison between suspended and dissolved fluxes, and 10Be analysis in the Nyong and Sanaga River basins, south Cameroon. Earth Surf. Process. Landf. 41, 1671–1683. https://doi.org/10.1002/esp.3939

Riebe, C.S., Granger, D.E., 2013. Quantifying effects of deep and near-surface chemical erosion on cosmogenic nuclides in soils, saprolite, and sediment. Earth Surf. Process. Landf. 38, 523–533. https://doi.org/10.1002/esp.3339

Riebe, C.S., Hahm, W.J., Brantley, S.L., 2017. Controls on deep critical zone architecture: a historical review and four testable hypotheses. Earth Surf. Process. Landf. 42, 128–156. https://doi.org/10.1002/esp.4052

Riebe, C.S., Kirchner, J.W., Finkel, R.C., 2003. Long-term rates of chemical weathering and physical erosion from cosmogenic nuclides and geochemical mass balance. Geochim. Cosmochim. Acta 67, 4411–4427. https://doi.org/10.1016/S0016-7037(03)00382-X

Salgado, A., Varajão, C., Colin, F., Braucher, R., Varajão, A., Nalini Jr, H., 2007. Study of the erosion rates in the upper Maracujá Basin (Quadrilátero Ferrífero/MG, Brazil) by the in situ produced cosmogenic10Be method. Earth Surf. Process. Landf. 32, 905–911. https://doi.org/10.1002/esp.1448

Scherler, D., DiBiase, R.A., Fisher, G.B., Avouac, J.-P., 2017. Testing monsoonal controls on bedrock river incision in the Himalaya and Eastern Tibet with a stochastic-threshold stream power model. J. Geophys. Res. Earth Surf. 122, 1389–1429. https://doi.org/10.1002/2016JF004011

Şengör, A.M.C., Lom, N., Polat, A., 2022. The nature and origin of cratons constrained by their surface geology. GSA Bull. 134, 1485–1505. https://doi.org/10.1130/B36079.1

Séranne, M., Bruguier, O., Moussavou, M., 2008. U-Pb single zircon grain dating of Present fluvial and Cenozoic aeolian sediments from Gabon: consequences on sediment provenance, reworking, and erosion processes on the equatorial West African margin. Bull. Société Géologique Fr. 179, 29–40.

Stone, J.O., 2000. Air pressure and cosmogenic isotope production. J Geophys Res 105, 23753–23759.

Suhrhoff, T.J., Rickli, J., Christl, M., Vologina, E.G., Pham, V., Belhadj, M., Sklyarov, E.V., Jeandel, C., Vance, D., 2022. Source to sink analysis of weathering fluxes in Lake Baikal and its watershed based on riverine fluxes, elemental lake budgets, REE patterns, and radiogenic (Nd, Sr) and 10Be/9Be isotopes. Geochim. Cosmochim. Acta 321, 133–154. https://doi.org/10.1016/j.gca.2022.01.007

Thiéblemont, D., Castaing, C., Billa, M., Bouton, P., Préat, A., 2009a. Notice explicative de la carte géologique et des ressources minérales de la République Gabonaise à 1/1000000. Programme Sysmin 8, 384.

Thiéblemont, D., Castaing, C., Bouton, P., Billa, M., Prian, J.P., Goujou, J.C., Boulingui, B., Ekogha, H., Kassadou, A., Simo Ndounze, S., Ebang Obiang, M., Nagel, J.L., Abouma Simba, S., Husson, Y., 2009b. Carte géologique et des Ressources minérales de la République Gabonaise à 1/1 000 000.

Uppala, S.M., KÅllberg, P.W., Simmons, A.J., Andrae, U., Bechtold, V.D.C., Fiorino, M., Gibson, J.K., Haseler, J., Hernandez, A., Kelly, G.A., Li, X., Onogi, K., Saarinen, S., Sokka, N., Allan, R.P., Andersson, E., Arpe, K., Balmaseda, M.A., Beljaars, A.C.M., Berg, L.V.D., Bidlot, J., Bormann, N., Caires, S., Chevallier, F., Dethof, A., Dragosavac, M., Fisher, M., Fuentes, M., Hagemann, S., Hólm, E., Hoskins, B.J., Isaksen, L., Janssen, P. a. E.M., Jenne, R., Mcnally, A.P., Mahfouf, J.-F., Morcrette, J.-J., Rayner, N.A., Saunders, R.W., Simon, P., Sterl, A., Trenberth, K.E., Untch, A., Vasiljevic, D., Viterbo, P., Woollen, J., 2005. The ERA-40 re-analysis. Q. J. R. Meteorol. Soc. 131, 2961–3012. https://doi.org/10.1256/qj.04.176

Vanacker, V., von Blanckenburg, F., Hewawasam, T., Kubik, P.W., 2007. Constraining landscape development of the Sri Lankan escarpment with cosmogenic nuclides in river sediment. Earth Planet. Sci. Lett. 253, 402–414. https://doi.org/10.1016/j.epsl.2006.11.003

Viers, J., Dupré, B., Braun, J.-J., Deberdt, S., Angeletti, B., Ngoupayou, J.N., Michard, A., 2000. Major and trace element abundances, and strontium isotopes in the Nyong basin rivers (Cameroon): constraints on chemical weathering processes and elements transport mechanisms in humid tropical environments. Chem. Geol. 169, 211–241. https://doi.org/10.1016/S0009-2541(00)00298-9

Weber, F., Gauthier-Lafaye, F., Whitechurch, H., Ulrich, M., El Albani, A., 2016. The 2-Ga Eburnean Orogeny in Gabon and the opening of the Francevillian intracratonic basins: A review. Comptes Rendus Geosci. 348, 572–586. https://doi.org/10.1016/j.crte.2016.07.003

Willenbring, J.K., Codilean, A.T., McElroy, B., 2013. Earth is (mostly) flat: Apportionment of the flux of continental sediment over millennial time scales. Geology G33918.1. https://doi.org/10.1130/G33918.1

Wittmann, H., Oelze, M., Gaillardet, J., Garzanti, E., Von Blanckenburg, F., 2020. A global rate of denudation from cosmogenic nuclides in the Earth's largest rivers. Earth-Sci. Rev. 204, 103147. https://doi.org/10.1016/j.earscirev.2020.103147

Wittmann, H., von Blanckenburg, F., Maurice, L., Guyot, J.-L., Filizola, N., Kubik, P.W., 2011. Sediment production and delivery in the Amazon River basin quantified by in situ–produced cosmogenic nuclides and recent river loads. GSA Bull. 123, 934–950. https://doi.org/10.1130/B30317.1

Supplementary Material

S1 ^{26}Al vs ^{10}Be (the "banana" plot)

Here we present a "banana" plot of the two samples for which ^{26}Al has been measured in addition to ^{10}Be (Figure S1). The position of the samples in the banana plot (Figure S1) indicates that these samples are partly made up of recycled material (Batéké Plateaux). However, the proximity of the samples to the "surface banana" on the graph (in black on) suggests that the proportion of this recycled signal is low. The recycled signal did not affect the erosion rates deduced from ^{10}Be by more than the equivalent of 0.5 x halftime in the worst case (BTK08-5), which would represent a bias close to 25% in the sense of an underestimation of denudation rates.

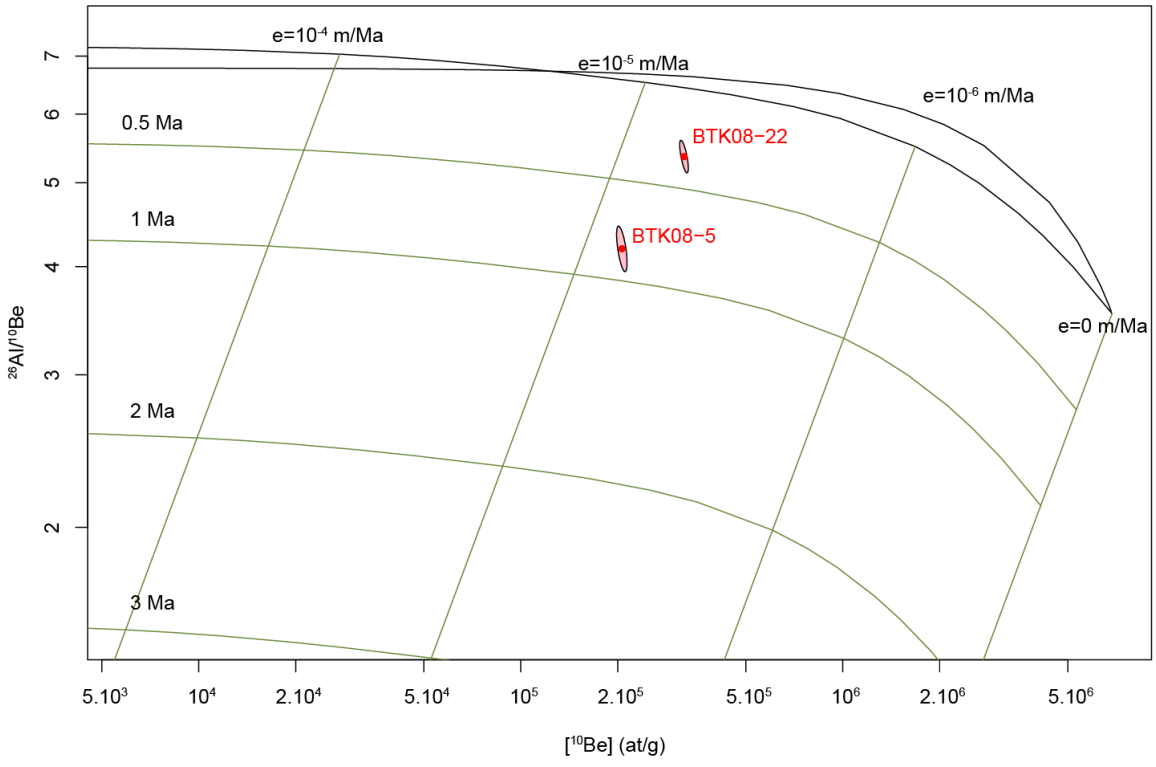

Figure S 1. Banana plot of ^{26}Al vs ^{10}Be data. The letter "e" represents the source erosion rate and the burial time is indicated (green lines). The "surface banana" is in black.

S2 ^{10}Be denudation rates in intermediate areas ("nested catchments")

In Figure S2, we present a map with intermediate areas for which we evaluated the denudation rates using the "nested catchment" method. At each sampling point, the denudation rates are converted into total denudation fluxes (denudation rate x area). A difference between two successive points indicates the flux of the material sourced from the area in-between; conversely, an average denudation rate can be calculated for this source area (denudation flux/area).

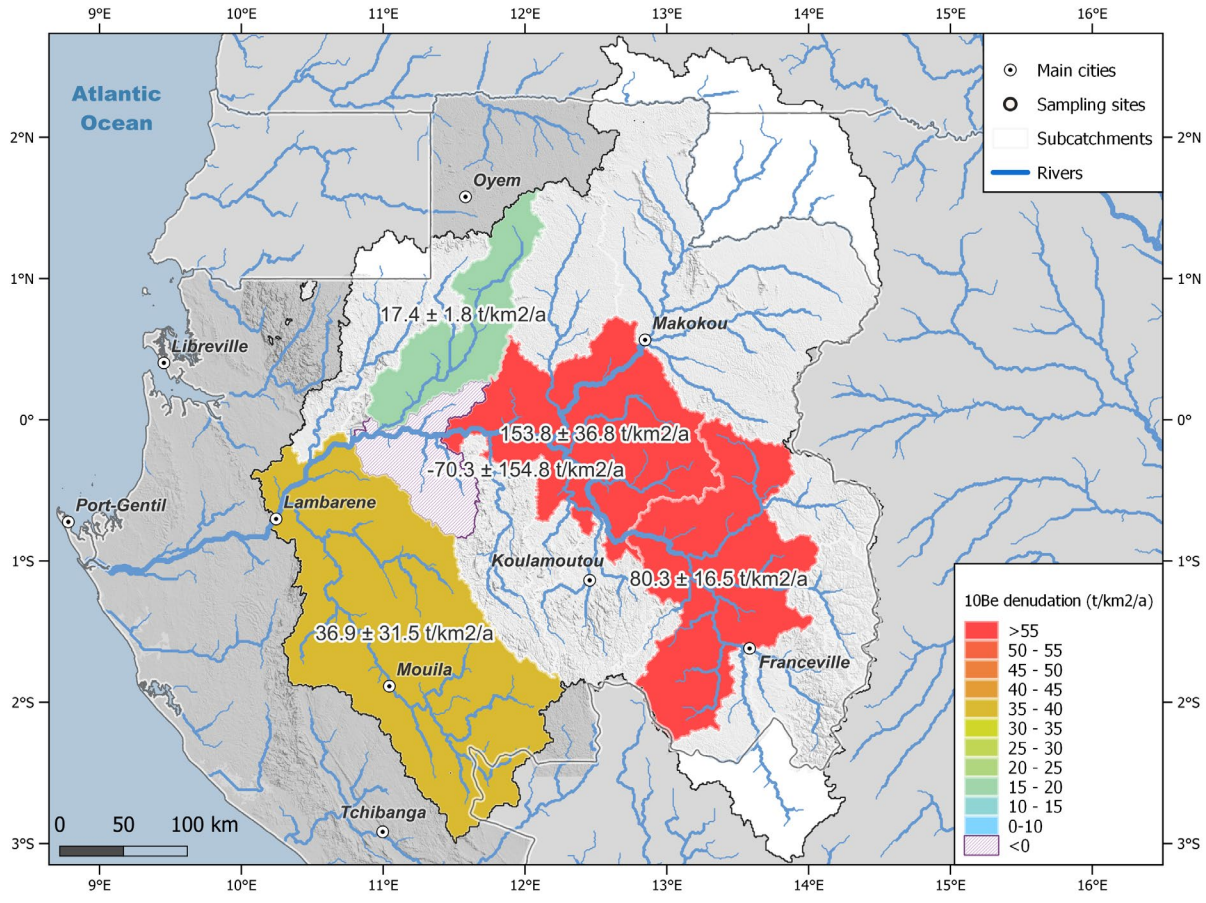

Figure S2. Colored scale map of the denudation rates for the "nested catchments" in the ORB, calculated as the difference in the estimated sediment flux between two successive stations along the Ogooué mainstream.

S3 ^{10}Be denudation rates *vs.* catchment area

Figure S3 represents the ^{10}Be denudation rate *vs.* the catchment area.

825

826

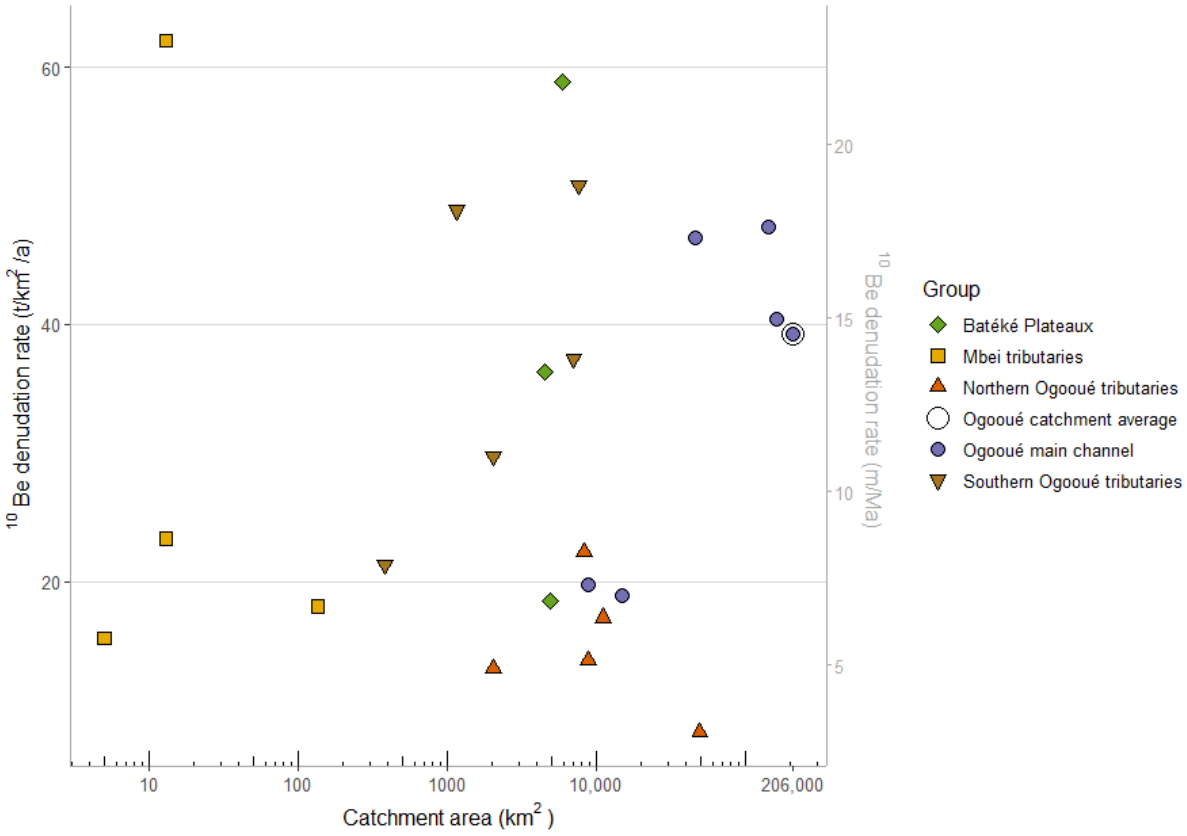

827

828 *Figure S3. [10]Be-derived denudation vs. catchment area.*

829

830

831

832

833